MID-AMERICA TRANSPORTATION CENTER

Report # MATC-UNL: 043

Final Report
WBS: 25-1121-0005-043

Evaluation of Concrete Models in LS-DYNA to Develop a MASH Test Level 6 (TL-6) Barrier System

Jennifer Rasmussen, Ph.D.
Associate Research Professor
Department of Civil and Environmental Engineering
University of Nebraska-Lincoln

Keyvan Zare Rami, Ph.D. student
Graduate Research Assistant
Department of Civil and Environmental Engineering
University of Nebraska-Lincoln

Yong-Rak Kim, Ph.D.
Professor
Zachry Department of Civil and Environmental Engineering
Texas A&M University

Shayan Gholami, Ph.D. student
Graduate Research Assistant
Zachry Department of Civil and Environmental Engineering
Texas A&M University

Ronald Faller, Ph.D.
Research Full Professor
Department of Civil and Environmental Engineering
University of Nebraska-Lincoln

2020

A Cooperative Research Project sponsored by
U.S. Department of Transportation- Office of the Assistant Secretary for Research and Technology

Evaluation of Concrete Models in LS-DYNA to Develop a MASH Test Level 6 (TL-6) Barrier System

Jennifer Rasmussen, Ph.D.
Associate Research Professor
Department of Civil and Environmental Engineering
University of Nebraska-Lincoln

Keyvan Zare Rami, Ph.D. Student
Graduate Research Assistant
Department of Civil and Environmental Engineering
University of Nebraska-Lincoln

Yong-Rak Kim, Ph.D.
Professor
Zachry Department of Civil and Environmental Engineering
Texas A&M University

Shayan Gholami, Ph.D. Student
Graduate Research Assistant
Zachry Department of Civil and Environmental Engineering
Texas A&M University

Ronald Faller, Ph.D.
Research Full Professor
Department of Civil and Environmental Engineering
University of Nebraska-Lincoln

A Report on Research Sponsored by

Mid-America Transportation Center

University of Nebraska–Lincoln

July 2020

Technical Report Documentation Page

1. Report No. 25-1121-0005-043	2. Government Accession No.	3. Recipient's Catalog No.
4. Title and Subtitle Evaluation of Concrete Models in LS-DYNA to Develop a MASH Test Level 6 (TL-6) Barrier System		5. Report Date July 2020
		6. Performing Organization Code
7. Author(s) Shayan Gholami[1], Keyvan Zare-Rami[2], Yong-Rak Kim[3] ORCID: 0000-0002-5421-750X, Jennifer Rasmussen[4] ORCID: 0000-0003-0909-0850, and Ronald Faller[5] ORCID: 0000-0001-7660-1572 [1,3]Texas A&M University, College Station, Texas 77843 [2,4,5]University of Nebraska-Lincoln, Lincoln, Nebraska 68583		8. Performing Organization Report No. 25-1121-0005-043
9. Performing Organization Name and Address Mid-America Transportation Center Prem S. Paul Research Center at Whittier School 2200 Vine St. Lincoln, NE 68583-0851		10. Work Unit No. (TRAIS)
		11. Contract or Grant No. 69A3551747107
12. Sponsoring Agency Name and Address Office of the Assistant Secretary for Research and Technology 1200 New Jersey Ave., SE Washington, D.C. 20590		13. Type of Report and Period Covered Final Report July 2018-July 2020
		14. Sponsoring Agency Code MATC TRB RiP No. 34760
15. Supplementary Notes		

16. Abstract

The concept design of the Manual for Assessing Safety Hardware (MASH) test level 6 (TL-6) safety barrier is configured with reinforced concrete material. Analysis and design of this barrier included use of a finite element software (i.e., LS-DYNA) to simulate the impact of laboratory-level samples and prototype structures. A reliable simulation depends on how accurately the nonlinear behavior of concrete is predicted under impact loading. The current version of LS-DYNA contains several constitutive material models that are specifically intended for predicting brittle deformation-fracture behavior of materials, such as concrete. The first part of this study consists of a literature review that investigates the viability of existing models for simulating the nonlinear behavior of concrete. The viable models are then further investigated in the second part of this project. Continuous Surface Cap Model (CSCM) and Karagozian & Case Concrete Model (K&C) in LS-DYNA were selected as candidate models and were evaluated and compared with experimental results. Simulation results showed that both models overall can predict the behavior of plain concrete, in both quasi-static and low-velocity impact tests. However, the responses of these models to compression, shear, or flexural stress were different. Compressive strength as the critical property of plain concrete was well matched by both models, while the post-failure behavior of the models was different. The acceleration-time curve in the low-velocity impact test also showed that the K&C model can predict the maximum positive and negative acceleration more accurately than CSCM, while the CSCM element erosion capability resulted in a deformation contour closer to reality.

17. Key Words MASH TL-6 Safety Barrier, LS-DYNA, Concrete Models, Continuous Surface Cap Model (CSCM), Karagozian & Case Concrete Model (K&C)	18. Distribution Statement		
19. Security Classif. (of this report) Unclassified	20. Security Classif. (of this page) Unclassified	21. No. of Pages 70	22. Price

Table of Contents

List of Figures

List of Tables

List of Abbreviations

Mid-America Transportation Center (MATC)
Midwest Roadside Safety Facility (MwRSF)
Nebraska Transportation Center (NTC)
Manual for Assessing Safety Hardware (MASH)
Test level 6 (TL-6)
Continuous Surface Cap Model (CSCM)
Karagozian & Case (K&C)

Disclaimer

Abstract

The concept design of the Manual for Assessing Safety Hardware (MASH) test level 6 (TL-6) safety barrier is configured with reinforced concrete material. Analysis and design of this barrier included use of a finite element software (i.e., LS-DYNA) to simulate the impact of laboratory-level samples and prototype structures. A reliable simulation depends on how accurately the nonlinear behavior of concrete is predicted under impact loading. The current version of LS-DYNA contains several constitutive material models that are specifically intended for predicting brittle deformation-fracture behavior of materials, such as concrete. The first part of this study consists of a literature review that investigates the viability of existing models for simulating the nonlinear behavior of concrete. The viable models are then further investigated in the second part of this project. Continuous Surface Cap Model (CSCM) and Karagozian & Case Concrete Model (K&C) in LS-DYNA were selected as candidate models and were evaluated and compared with experimental results. Simulation results showed that both models overall can predict the behavior of plain concrete, in both quasi-static and low-velocity impact tests. However, the responses of these models to compression, shear, or flexural stress were different. Compressive strength as the critical property of plain concrete was well matched by both models, while the post-failure behavior of the models was different. The acceleration-time curve in the low-velocity impact test also showed the K&C model can predict the maximum positive and negative acceleration more accurately than CSCM, while the CSCM element erosion capability resulted in a deformation contour closer to reality.

Chapter 1 Introduction

1.1 Problem Statement

Barriers that meet the American Association of State Highway and Transportation Officials (AASHTO) Manual for Assessing Safety Hardware (MASH) Test Level (TL) 4 or 5 standards are utilized in locations that experience a large volume of trucks. Unfortunately, while these designs are appropriate for tractor trailers, they do not meet TL-6 standards, which apply to tanker trucks. To date, only one TL-6 vehicle containment system has been developed, but cost issues have prevented its widespread implementation. Consequently, critical infrastructure (i.e., bridge abutments) are not protected against tanker truck crashes, which places critical facilities (e.g., schools, hospitals) at risk of exposure to hazardous materials after a crash. To address this issue, a new, cost-effective, and structurally adequate TL-6 safety barrier system needs to be developed. The design of the MASH TL-6 safety barrier system is most likely configured with reinforced concrete materials; additionally, a finite element software (e.g., LS-DYNA) is used to simulate the impact of small component concrete samples that can be used to design the full-scale barrier system. Among the various aspects that need to be considered during development, selection of a proper constitutive material model and model parameters is one of the essential components, because the material model and model parameters used in computational simulation can significantly affect the time and costs of barrier design without compromising predictive power. Thus, it is critical to identify the proper constitutive model and model parameters for simulation of the barrier system. Concrete displays several characteristic responses under various loading scenarios, such as pre- and post-peak dilatancy, pre-peak hardening, post-peak softening, strain rate enhancement, and damage. LS-DYNA provides several constitutive models that are intended to capture those unique features. In order to select the proper material model and model

parameters, the various models in LS-DYNA need to be examined. After selecting candidate constitutive models, an appropriate set of experimental tests needs to be selected and subsequently used for model validation. Viable models are then further investigated through comparisons with the experimental results, which enables improved selection of material models used in the analysis of the TL-6 barrier.

1.2 Relevance to MATC Theme and Thematic Thrust Areas

The theme of MATC is to improve safety and minimize risk associated with increasing multi-modal freight movements within the U.S. surface transportation system. States that are part of Region VII experience a considerable amount of freight traffic on their roadways. In order to minimize the effects of additional freight traffic on the traveling public, transportation infrastructure, and the region's economy, TL-6 barriers could be placed in critical areas to prevent accidents involving hazardous tractor tank trailers from becoming catastrophic. Cost and material usage have largely prevented current TL-6 barriers from widespread implementation. However, development of a new, cost-effective TL-6 barrier may facilitate its deployment to critical areas that may help to prevent catastrophic accidents, which would ultimately affect the traveling public, infrastructure, and the region's economy. One of the core inputs into the development of the TL-6 barrier is a concrete material model that can be used in the LS-DYNA simulations.

1.3 Research Approach and Methods

The first part of this project is a review of the literature regarding existing models that are used in simulations of the nonlinear behavior of concrete under quasi-static and impact loading. This review also investigates the experimental tests that are available in the Midwest Roadside Safety Facility (MwRSF) and any further required tests (for validation) from the literature. In the

second part of this project, model simulations are integrated with test results to evaluate and validate materials models in the LS-DYNA. The specific objectives of this project are as follows:

- To introduce the theory behind plastic-damage based models (CSCM and K&C);
- To conduct a parametric analysis for evaluating the effects of model input parameters and loading rate on the mechanical behavior of concrete;
- To review the experimental tests that include concrete behavior under quasi-static and impact loading;
- To evaluate the effectiveness of the CSCM and K&C concrete models for simulating the nonlinear behavior of concrete under quasi-static and impact loading by comparing the simulation results with the experimental results; and
- To provide a summary of the results and derive conclusions regarding the viability of the CSCM and K&C models for predicting the nonlinear behavior of concrete.

Chapter 2 Background

For many years, modeling of concrete behavior has been a challenging task, as it exhibits nonlinear and damage behavior at various loading types and conditions. Concrete is a complex heterogeneous material that is a mixture of randomly distributed aggregates within a cementitious paste. Concrete exhibits non-linear and anisotropic damage due to its complex microstructure, the properties of its individual components, and the unique characteristics of the aggregate-paste interface. The phenomenology of the concrete damage process and post-damage behavior arise from two mechanisms: development of localized microcracks and slip-type plastic flow.

The heterogeneous nature of concrete creates a nonuniform stress distribution under loading. Microcracks typically nucleate and propagate within areas where stiffness is relatively low and the stress concentration is sufficiently high to create microcracks. Prior to the complete failure of concrete, the formation of microcracks creates a weak band of weaker stiffness as compared to neighboring material. Eventually, increases in loading can cause microcracks to coalesce that results in formation of discrete cracks. Generally, in ordinary concrete mixtures, the interface between aggregates and paste is prone to localized band development and crack propagation, while in high strength concrete, cracks tend to go through aggregates. Any local opening or sliding deformation of the localized band is unrecoverable, which causes plastic strain. Similar to other granular materials, experimental results show that the plastic deformation of concrete does not necessarily follow the traditional associated flow rule (Nemat-Nasser and Shokooh 1980).

A sound model should be able to accurately capture basic phenomenological responses of concrete, in particular the degradation of anisotropic stiffness and plastic response due to the

development of localized microcracks under various loading conditions such as quasi-static and impact loadings (Ortiz 1985). However, developing purely mechanics-based models for capturing the complex behavior of concrete is quite challenging. Hence, many researchers have attempted to drive phenomenological constitutive models in order to reproduce the observed response of concrete. However, these models are typically limited in their ability to accurately predict the response of different types of concrete across a broad range of applications and loading scenarios (Buyukozturk and Shareef 1985; Liu, Lü, and Guan 2007).

On the other hand, several mechanics-based constitutive models have been published over the past decades. They have shown promising capabilities to reproduce nonlinear responses of concrete (Yonten et al. 2005). A nonlinear response includes key characteristic behavior of concrete at different stages of loading such as the initial elastic response, plastic deformation, and damage process (Liu, Lü, and Guan 2007). Constitutive models that potentially meet these characteristics are plasticity-damage models derived by integrating plasticity and damage models. Plasticity models are generally based on a yielding surface and a flow rule. A yielding surface defines the limits of the elastic state. When the state of stress reaches the yielding surface, plastic deformation can occur. However, the shape and size of the yield surface may change as plastic deformation evolves. Degradation of yield strength is typically represented by a damage growth parameter, D. Typically, a mathematical function defines the damage rate, D, in terms of the current state of variables such as damage, stress, elastic strain, or plastic strain. The evolution of yielding surface is governed by a hardening rule. The flow rule describes the relationship between increments of plastic strain and stress (Lubliner et al. 1989). There are two types of flow rules: associated and non-associated flow rules. The flow rule is associated with plasticity if the gradient of plastic potential flow is normal to the yield surface. However, in

nature, this is not always the case, especially for granular materials such as soils and concrete. Therefore, the non-associated flow rule is more appropriate when the plastic strain rate is not perpendicular to the yield surface.

Among all available plasticity constitutive models, a few that are suitable for concrete simulation have been implemented into LS-DYNA. Some of these models are based on the associated flow rule: the geologic cap (MAT_25), continuous surface cap (MAT_145), continuous surface cap concrete, CSCM (MAT_159), and Riedel-Hiermaier-Thoma (MAT_272), to name a few. On the other hand, other models adopted the non-associated flow rule when the plastic potential function is different from yield surface (Hallquist 2013). There is a special case of non-associated models where the von Mises criterion is employed as the plastic potential function. These models use Prandtl–Reuss flow theory to calculate plastic strain, including K&C (MAT_72R3), Winfrith (MAT_84/85), and Johnson Holmquist (MAT_111).

Almost all the aforementioned models are capable of predicting key features of concrete behavior, such as pre-peak hardening, post-peak softening, and dilatancy. However, some of these models have become more popular than others for applications in engineering due to either the simplicity of the model (MAT_72, MAT_84/85, and MAT_111) or being internally calibrated for concrete (MAT_72R3 and MAT_159) (Jiang and Zhao 2015). For example, MAT_72R3 and MAT_159 require nearly 50 and 40 user defined parameters, respectively, while LS_DYNA contains an internal parameter generator that can create those parameters based merely on unconfined compressive strength and maximum aggregate size (Hallquist 2013). Over the last several years, a considerable amount of research that evaluated commercially available software (in particular LS-DYNA) has been conducted. These studies investigated the performance of concrete models in a wide range of applications, ranging from plain concrete

component tests to reinforced concrete structure tests (Jiang and Zhao 2015). With a few exceptions, most studies focused on the behavior of reinforced concrete structural elements under impact loading.

Borrvall and Riedel used the RHT model to simulate a reinforced concrete plate subjected to a blast (Borrvall 2009). Comparison of the damage profile showed the simulation and the physical test were in good agreement; however, the model was unable to adequately capture spalling. In another study, the Winfrith model was used to simulate a reinforced concrete slab under blast loading. The Winfrith model accounts for reinforcement of concrete implicitly within the constitutive model. The result showed that the Winfrith model overestimated slab deformation as compared to the actual test (L. Schwer 2014). The accuracy of the K&C model was extensively investigated by analyzing the results of concrete simulation for various scenarios with complex geometries and different loading conditions such as impact, blast, triaxial compression, and uniaxial tension. In most cases, the K&C model was able to capture the key features of plain and reinforced concrete; however a few potential improvements such as non-isotropic cracking and shear dilatancy were proposed (Crawford et al. 2012).

In a comprehensive study, (Murray 2004) evaluated performance of MAT_159 (CSCM model) by simulating various tests such as drop tower and bogie vehicle impact. It was found that the CSCM model accurately predicted peak loads, maximum deformation, and damage contours as compared to the experiments. They extended evaluation by simulating the impact between pendulum and a reinforced concrete railing and compared the results to the experiment. The velocity time-history data and damage contour showed an acceptable agreement with the experimental result (Abu-Odeh 2006).

Although an overview of the relevant literature indicates a general agreement between model simulation and experimental result for reinforced concrete structures, questions remain regarding how the models perform for plain concrete samples. The lack of reinforcement may influence the simulation results. A comprehensive study performed at MwRSF investigated the accuracy of the K&C, RHT, and CSCM models for predicting the behavior of plain concrete under compression, shear, tension, and flexural loading cases (Winkelbauer et al. 2016). It was found that the K&C and CSCM models made reasonably better predictions than other models when were compared to the experimental results.

Concrete structures are often subjected to dynamic loads in the real-world. However, in practice, the majority of tests that are designed to characterize the basic properties of concrete are quasi-static and require a less complex test setup and generate results that are less stochastic. Explicit analysis is often used when dynamic equilibrium governs the problem, such as impact loading and blast loading scenarios. In such conditions, the strain rate is typically high and plays an important role in material behavior. On the other hand, the implicit method should be used when static equilibrium can describe the problem. Such events happen at much slower loading rates in which strain rates have minimal effects on material behavior. Since the approach of these two solutions are inherently different, there are questions regarding how different concrete models perform in the implicit solution compared to the explicit solution. The majority of previous studies only investigated the performance of concrete models using explicit solvers, while only a few studies have been published that used the implicit approach.

Chapter 3 Experimental Studies

This chapter summarizes the experimental studies that were performed in order to compare with the model simulation results. For the quasi-static tests, Midwest Roadside Safety Report TRP-03-330-16 (Winkelbauer et al. 2016) was employed. Also, for the impact test, the study conducted by (Yilmaz et al. 2014) was selected, which provided sufficient input details for a finite element simulation. All tests were performed on plain concrete samples.

3.1 Uniaxial Compressive Strength Test

Based on (Winkelbauer et al. 2016), uniaxial compressive strength tests were conducted per ASTM C39 using 4 x 8 inches plain concrete cylinders, as shown in figure 3.1. Average compressive strength was determined using results from seven replicates. A load cell located on the testing apparatus captured the force data while a laser extensometer captured displacements. Testing was conducted in a load-control setup with 35 psi/sec (0.25 MPa/sec) until the failure point was reached. Engineering axial stress versus engineering axial strain are plotted in figure 3.2; additionally, the results are summarized in table 3.1. The average compressive strength was 9.07 ksi (62.5 MPa) and the average failure strain was 0.0025. Failure strain values were higher for tests 2 and 3 with the same peak stress, which are considered outliers. The excessive amount of noise observed in the results is primarily due to issues with the resolution of the laser extensometer. However, the overall stress-strain behavior was well captured by the testing setup.

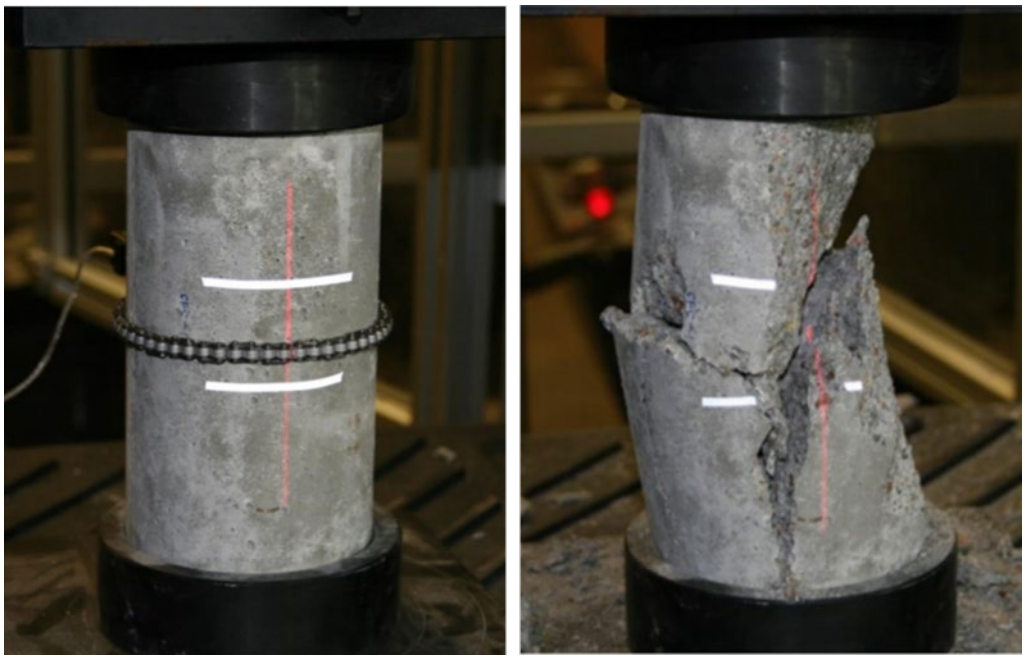

Figure 3.1 Uniaxial compressive strength setup: before and after failure (Winkelbauer et al. 2016).

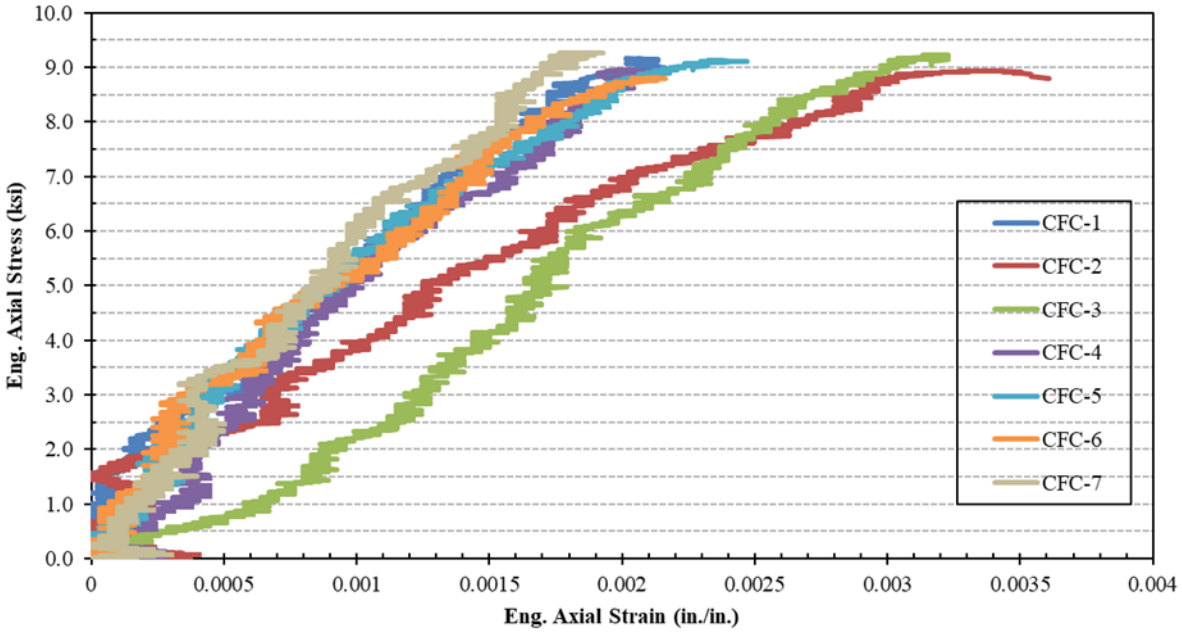

Figure 3.2 Summary of the engineering axial stress-strain curve (Winkelbauer et al. 2016)

Table 3.1 Summary of uniaxial compressive strength test results (Winkelbauer et al. 2016)

Test No.	Peak Eng. Stress [ksi]	Elastic Modulus [ksi]	Failure strain
1	9.16	4234.96	0.00216
2	8.93	2475.70	0.00361
3	9.23	2858.93	0.00323
4	8.96	4241.95	0.00211
5	9.12	3694.51	0.00247
6	8.80	4064.12	0.00217
7	9.27	4803.58	0.00193

3.2 4-Point Bending Test

Based on Winkelbauer et al. 2016, 4-point bending tests (fig 3.3 and fig 3.4) were conducted with different support spans, ranging from 9 to 18 inches, while the top rollers had a fixed spacing of 6 inches. The narrower span can evaluate the shear behavior of concrete, while the wider span accounts for flexural failure. Specimens included six beams made of plain concrete with no reinforcement with dimensions of 6 x 6 x 22 inches. Two different types of strain gauges were used to capture surface strain: linear and 0-45-90-degree orientation rosettes. The strain summary is presented in table 3.3, table 3.4, and figure 3.5. String potentiometers captured the vertical deflection at different locations. Force values were recorded from the load cell on top. All tests were conducted in displacement control mode of 0.0003 in./sec (0.00762 mm/sec), except test No. 4 that had a lower ratio of 0.0001 in./sec (0.00254 mm/sec). A summary of all tests is shown in table 3.2. In this study, test results of the two support spans (9 inches and 18 inches) were used for model simulations, which represent shear and flexural failure, respectively.

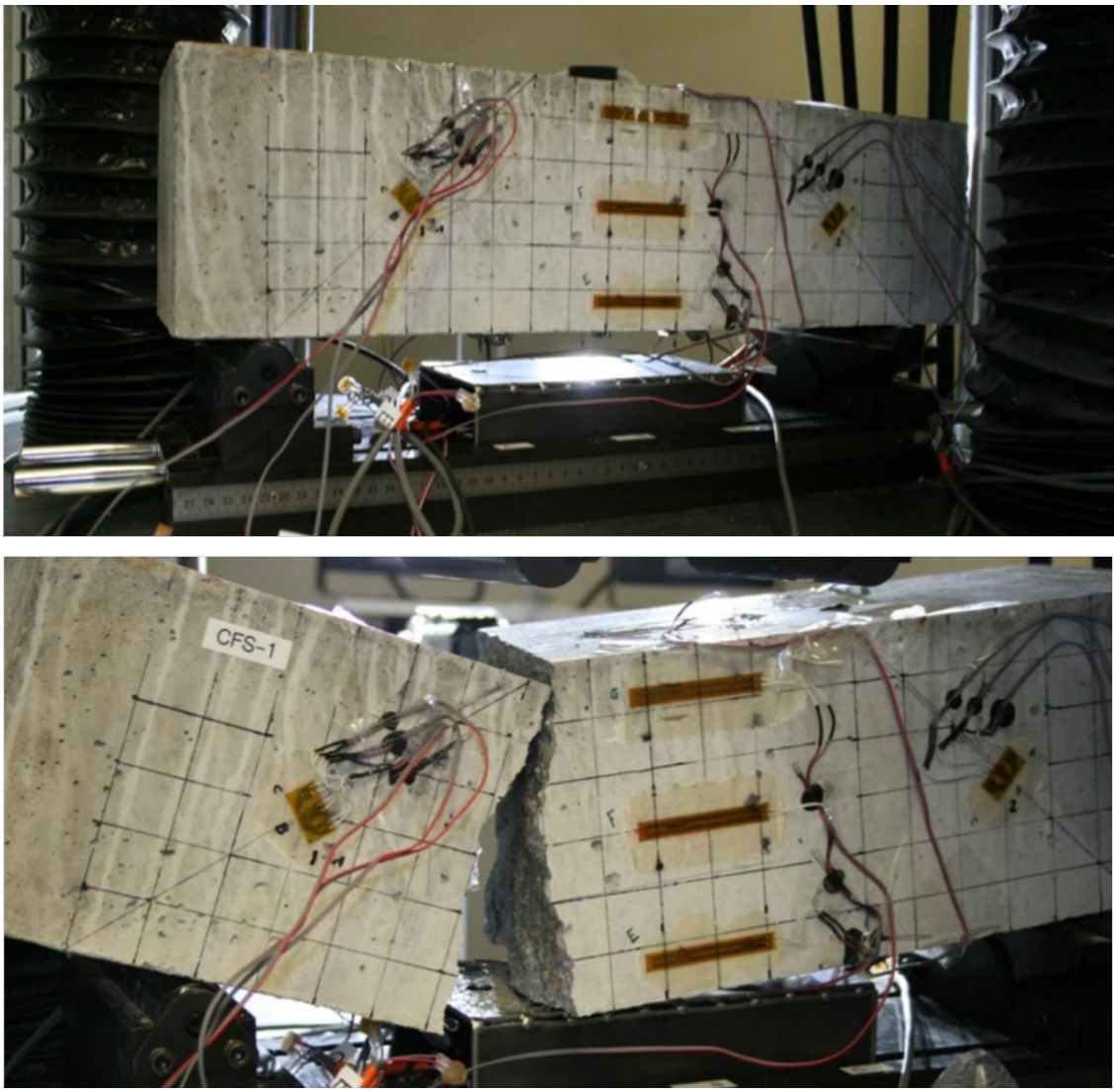

Figure 3.3 4-point bending test setup, sample with a span of 18 inches: before and after failure (Winkelbauer et al. 2016).

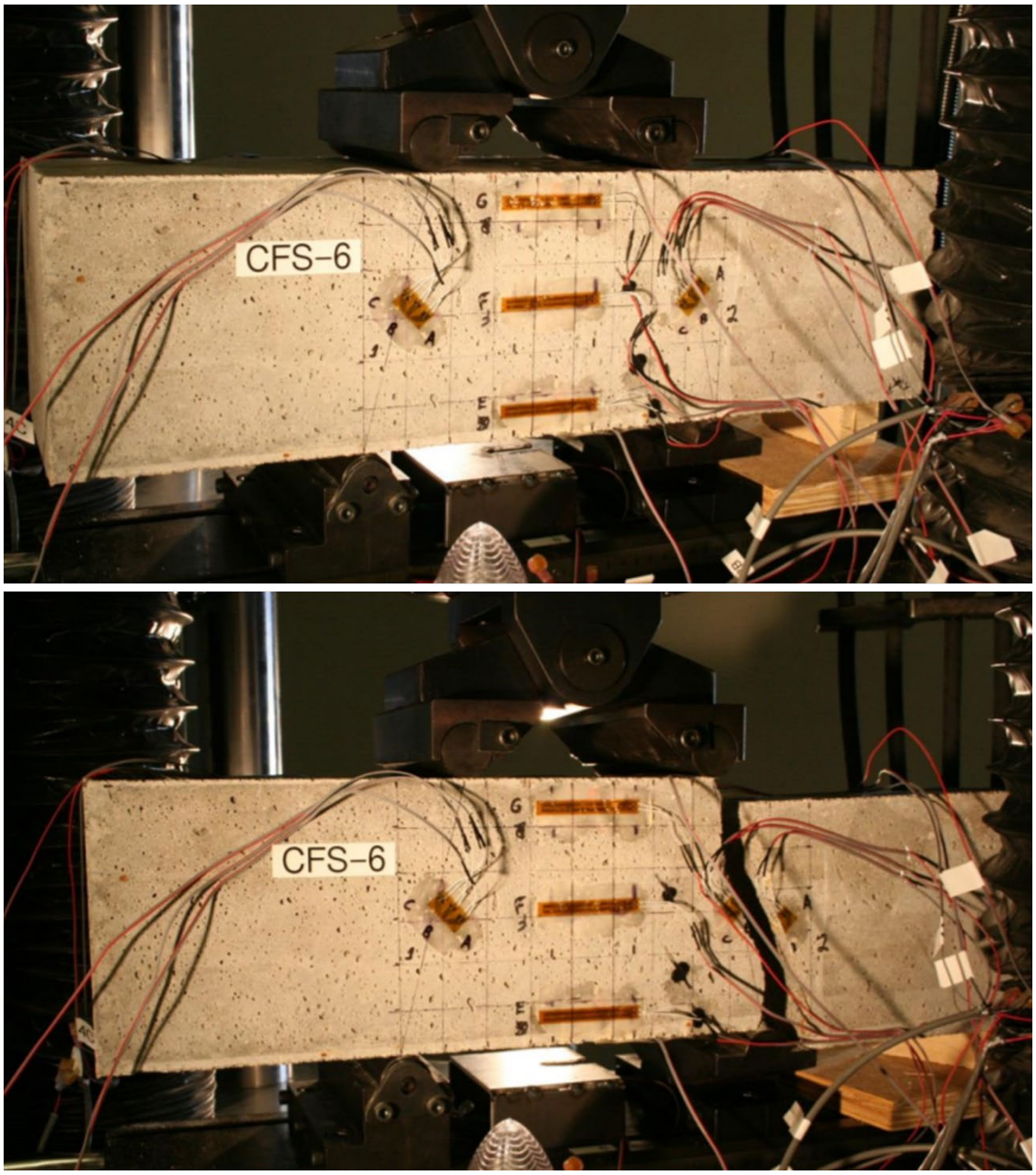

Figure 3.4 4-point bending test setup, sample with a span of 9 inches: before and after failure (Winkelbauer et al. 2016).

Table 3.2 Summary of 4-point bending test results *(Winkelbauer et al. 2016)*

Test No.	**Loading Rate** *in./s*	**Span Length** *in.*	**Fracture Pattern** -	**Max Load** *kip*
CFS-1	0.0003	18	Flexure	5.79
CFS-2	0.0003	12	Flexure	14.29
CFS-3	0.0003	10	Shear	16.88
CFS-4	0.0001	11	Flexure	16.92
CFS-5	0.0003	10	Flexure	18.98
CFS-6	0.0003	9	Shear	39.77

Table 3.3 4-point bending test, rosette gauges strain summary for the 18 inches span (Winkelbauer et al. 2016).

Gauge	Normal Strain, ε_x, @ Failure *in./in.*	Estimated Max./Min. Principal Strain		Estimated Max./Min. Principal Stress		Estimated γ_{max} *in./in.*	Estimated τ_{max1} *psi*	Estimated τ_{max2} *psi*	Estimated Principal Angles, θ_{1p} & θ_{2p} *degrees*	Estimated Shear Angles, θ_{1s} & θ_{2s} *degrees*
		ε_1 *in./in.*	ε_2 *in./in.*	σ_1 *psi*	σ_2 *psi*					
2A	1.22E-06	4.04E-05	-2.70E-05	177.5	-104.9	6.69E-05	135.4	135.9	135, 45	180, 90
2B	-2.60E-05									
2C	9.30E-06									
4A	-4.51E-06	8.64E-05	-8.94E-05	346.6	-364.7	1.76E-04	355.7	135.9	135, 45	180, 90
4B	-8.91E-05									
4C	1.14E-06									

Table 3.4 4-point bending test, rosette gauges strain summary for the 9 inches span (Winkelbauer et al. 2016).

Gauge	Normal Strain, ε_x, @ Failure *in./in.*	Estimated Max./Min. Principal Strain		Estimated Max./Min. Principal Stress		Estimated γ_{max} *in./in.*	Estimated τ_{max1} *psi*	Estimated τ_{max2} *psi*	Estimated Principal Angles, θ_{1p} & θ_{2p} *degrees*	Estimated Shear Angles, θ_{1s} & θ_{2s} *degrees*
		ε_1 *in./in.*	ε_2 *in./in.*	σ_1 *psi*	σ_2 *psi*					
4A	-1.40E-04	9.16E-05	-1.51E-04	315.7	-667.6	2.43E-04	490.7	828.6	105, 15	150, 60
4B	-7.71E-05									
4C	8.15E-05									

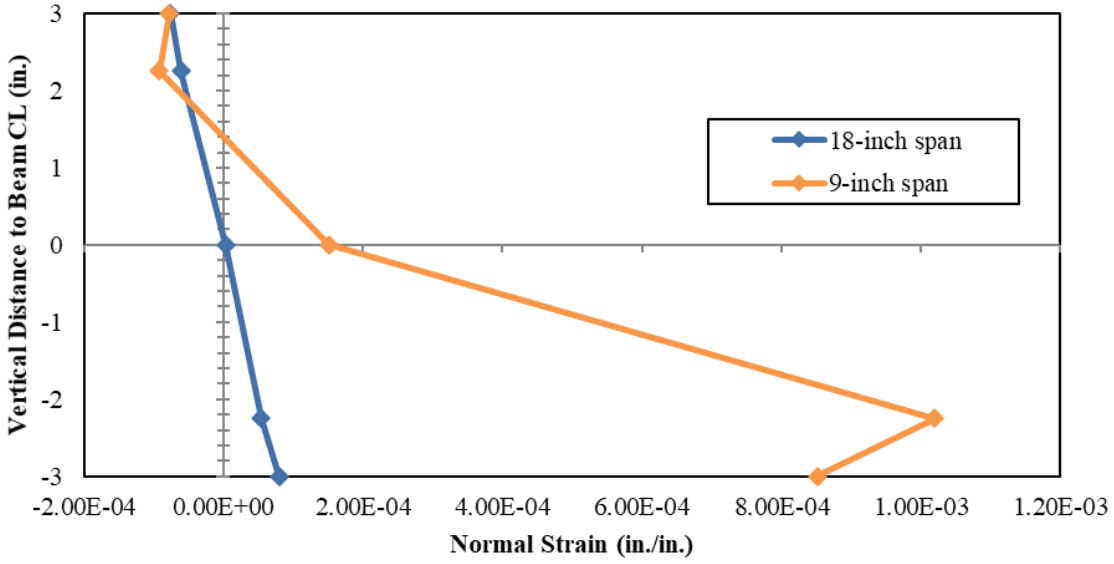

Figure 3.5 4-point bending test-linear strain distribution along the axis modified from (Winkelbauer et al. 2016).

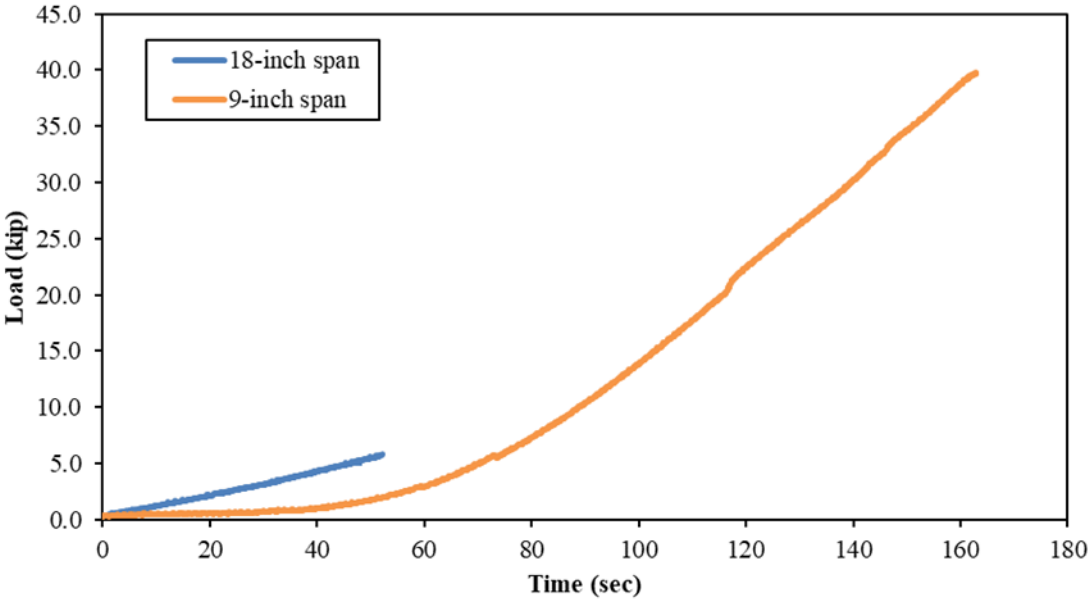

Figure 3.6 4-point bending test-force versus time plots (Winkelbauer et al. 2016).

3.3 Drop Weight Impact Test

Based on (Yilmaz et al. 2014), the low-velocity impact test was conducted by using a drop weight (fig. 3.7). As the behavior of concrete under quasi-static and impact loads is different, it is important to investigate concrete response at different loading regimes. The drop weight impact test was performed on six plain concrete beam specimens (150 x 150 x 710 mm). Compressive strength of the plain concrete was approximately 25 MPa, and a maximum aggregate size was 15 mm (fig. 3.8). The impactor was a steel hammer weighing approximately 5.25 kg, which was dropped on the center of the beam from different heights (from 300 mm to 500 mm). The shape of the impactor can induce a significant effect on the results of the impact due to any potential eccentricity. In order to avoid such an issue, a steel plate (50 x 150 x 15 mm) was pinned on the top of the beam at the location of impact to distribute the load uniformly over the surface. To capture the progress of acceleration, two accelerometers were mounted on the top of the beam with 150 mm spacing from the midspan of the impact.

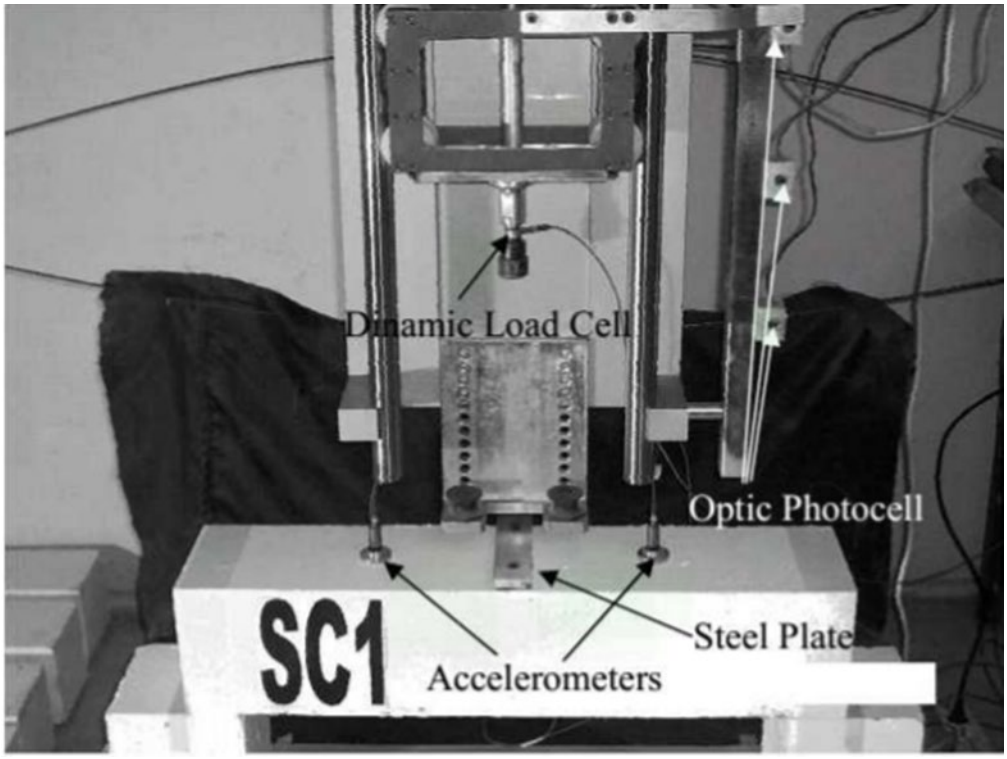

Figure 3.7 Drop weight impact setup (Yilmaz et al. 2014)

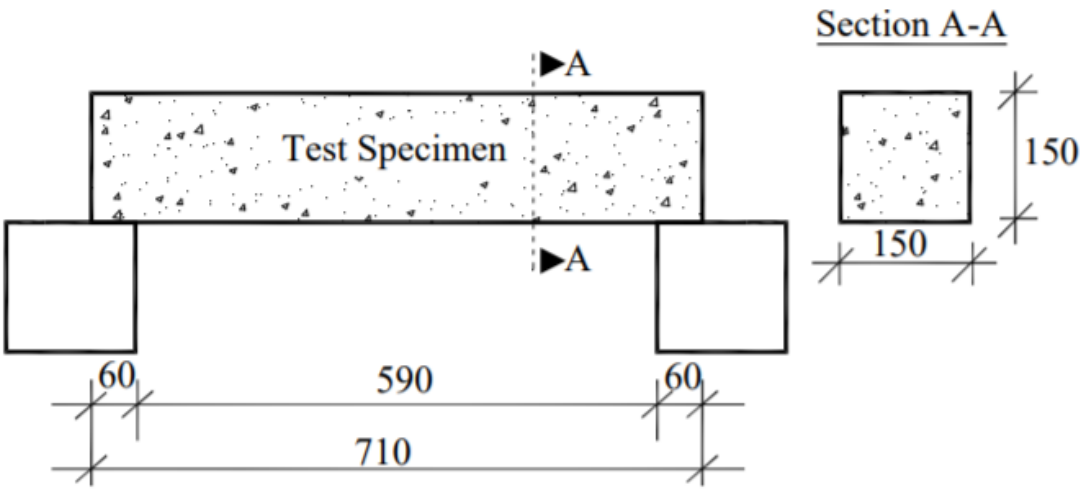

Figure 3.8 Drop weight impact test, specimen dimensions *(Yilmaz et al. 2014)*

The load-displacement curve resulting from the impact test with a drop height of 300 mm is shown in fig. 3.9. Only a limited range of the displacement was captured through the gauges in the test; hence, only the peak point could be used to compare with the model simulation results.

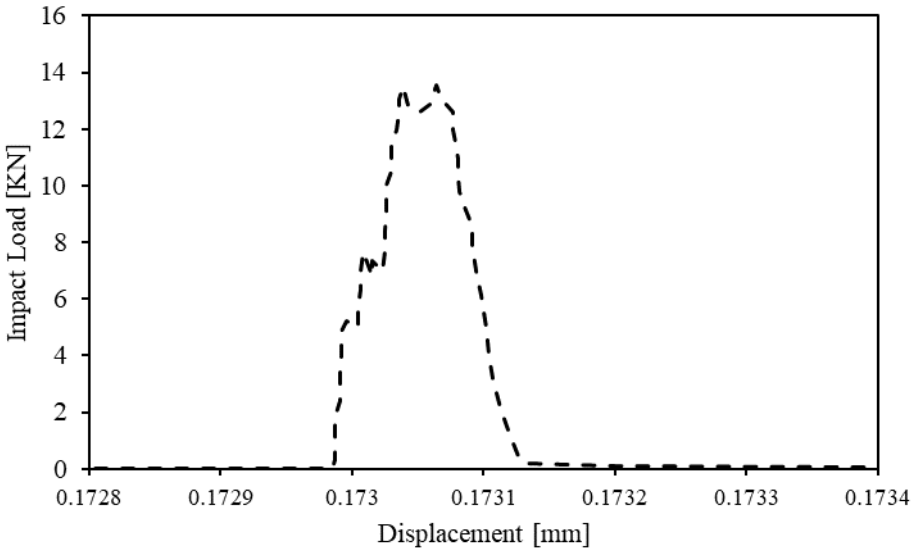

Figure 3.9 Drop weight impact test with a drop height of 300 mm: load-displacement curve (Yilmaz et al. 2014)

Different drop heights caused different accelerations results. A summary of the maximum positive and negative acceleration is shown in table 3.5. By increasing the drop height, the accelerations were more or less increased. However, due to the limited number of replicates, only the range of accelerations was used in the model validation process.

Table 3.5 Summary of drop weight impact test result: maximum positive and negative acceleration (Yilmaz et al. 2014).

	Maximum Acceleration [m/s^2]	
Drop Height [mm]	**Negative**	**Positive**
300	-2098.7514	1406.8521
350	-1724.8923	1735.8795
400	-1515.7431	1543.9959
450	-2590.821	1555.3755
500	-2537.5527	1550.8629

Chapter 4 Concrete Model Description

The unique behavior of plain concrete under quasi-static and impact loadings includes the formation and propagation of microcracks when the level of strain is high enough. With increased loading, these microcracks grow and coalesce, resulting in the formation of a macrocrack. Typically, in the compression, cracks occur parallel to the loading direction, while in the tension, cracks occur orthogonal to the load. When cracks form, additional loading makes the material unstable; this point is called the peak load (Brannon and Leelavanichkul 2009). Unlike metals, only a single parameter (i.e., uniaxial unconfined compressive strength) describes both the elastic and plastic responses of plain concrete and should include shear and tensile failures as well as compressibility (L. E. Schwer 2005). This single parameter cannot accurately represent the behavior of this complex material. Several material models have been proposed for thoroughly characterizing plain concrete based on three main approaches: discrete crack model, smeared crack model, and plasticity-damage models (Salamon and Harris 2014). Plasticity-damage models are suitable for modeling the properties of concrete under different loading conditions, of which two are discussed below. These two models have been frequently used, although they both have flaws in the generalized isotropic plasticity theory (Brannon and Leelavanichkul 2009).

4.1 Continuous Surface Cap Model

4.1.1 Theoretical Description

Continuous Surface Cap Model (CSCM) is an elastoplastic damage-based model that has been widely used for simulations of concrete structures under impact and dynamic loadings. This model is based on a continuum damage model introduced by Simo and Ju (1989). A brief theory of the CSCM model is presented below (Murray 2004; Jiang and Zhao 2015). The main features

of the CSCM model include:

- a yield surface defined by three stress invariants
- a hardening cap that expands and contracts
- plasticity-damage softening
- strain-rate dependency

The yield surface of the CSCM model is composed of two parts: the shear failure surface and a hardening cap, which are attached to each other by a smooth transition surface, as shown in figure 4.1(b). The yield surface of the CSCM is defined by the following function:

$$f(J_1, J_2', J_3', \kappa) = J_2' - \Re^2 F_f^2 F_c \qquad (4\text{-}1)$$

where:

$J_1, J_2', and\ J_3'$ = three stress invariants as defined by $J_1 = \sigma_{ii}, J_2' = S_{ij}S_{ij}/2$ (while the deviator stress tensor is defined by $S_{ij} = \sigma_{ij} - \sigma_{ii}\delta_{ij}/3$), and $J_3' = S_{ij}S_{jk}S_{ki}/3$,

κ = cap hardening parameter (Rubin 1991),

F_f = shear failure surface,

F_c = hardening cap surface, and

$\Re$ = Rubin scaling factor.

Multiplying shear failure surface by cap surface allows a smooth transition to occur from shear failure surface to cap surface. This smooth transition improves the stability of the model.

The yield surface at tensile and low confining pressure regime is defined by the shear failure surface. The equation of shear failure surface in the meridian plane is given by:

$$F_f(J_1) = \alpha - \gamma e^{-\beta J_1} + \theta J_1 \tag{4-2}$$

where $\alpha, \gamma, \beta, and\ \theta$ are the parameters of the model.

When the stress state is at a high confining pressure regime, the cap function is defined as follows:

$$F_c(J_1, \kappa) = 1 - \frac{(J_1 - L(\kappa))(|J_1 - L(\kappa)| + J_1 - L(\kappa))}{2(X(\kappa) - L(\kappa))^2} \tag{4-3}$$

where $X(\kappa)$ is the intersection of the cap surface with the J_1 axis and $L(\kappa)$, and is defined by:

$$X(\kappa) = \begin{cases} \kappa & if\ \kappa > \kappa_0 \\ 0 & otherwise \end{cases}$$

Plastic volume compaction and expansion are simulated by the cap surface movement. The movement of the cap is governed by the hardening rule, which is expressed by:

$$\epsilon_v^p = W \times (1 - e^{-D_1[X(\kappa) - X_0] - D_2[X(\kappa) - X_0]^2}) \tag{4-4}$$

where:

ϵ_v^p = plastic volumetric strain due to change in porosity,

W = maximum plastic volumetric strain,

X_0 = initial abscissa intercept of the cap surface, and

D_1 *and* D_1 = model parameters.

The Rubin scaling function, $\mathfrak{R}$, determines the material strength for any state of stress by scaling down the TXC (triaxial compression) shear strength, $\mathfrak{R}F_f$ (Rubin 1991). The Rubin function reshapes the yield surface from a circle to a hexagonal in the deviatoric plane, as shown in figure 4.1 (c).

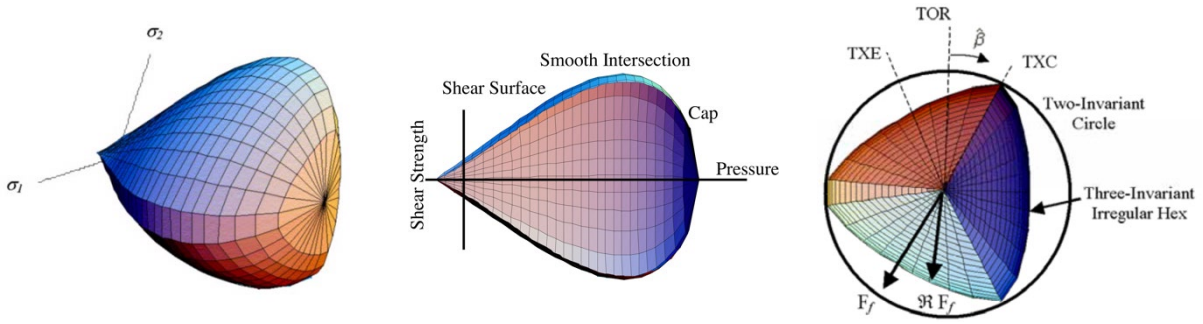

(a) Principal stress space *(b) Meridian section* *(c) Deviatoric section*

Figure 4.1 Different views of CSCM yield surface *(Murray 2004)*

4.1.2 Implementation in LS-DYNA

The CSCM model was implemented in LS-DYNA in 2004 (Murray 2004) as the keyword MAT_CSCM. The model is equipped with the following features:

- Element erosion based on the damage value
- Automated model parameter generation for concrete

To activate automated model parameter generation, the user selects the option CONCRETE (MAT_CSCM_CONCRETE). Next, LS-DYNA generates a set of CSCM model properties based on only two input values specified by the user: the unconfined compressive strength (f_c') and the maximum aggregate size (D_{max}). LS-DYNA uses model properties that are obtained by fitting to data for unconfined compressive strengths of 20 to 58 MPa (with emphasis on 28 to 48 MPa) and maximum aggregate sizes of 8 to 32 millimeters (Murray 2004). The users can also input their own material properties by selecting the *blank* option (MAT_CSCM).

4.2 Karagozian & Case (K&C) Concrete Model

4.2.1 Theoretical Description

The K&C concrete model or concrete damage model was developed by Javier Malvar (Malvar et al. 1994), primarily for analyzing concrete structures subjected to blast loading. A brief theory of the K&C concrete model is presented in this section (Markovich, Kochavi, and Ben-Dor 2009; Brannon and Leelavanichkul 2009).

The K&C concrete model employs a linear isotropic hypoelastic-plastic formulation and includes the effects of damage and strain rate. In regard to deviatoric stress tensors, it uses three shear strength surfaces that are called yield, limit, and residual surfaces, as follows:

$$Y_y = \Delta\sigma_y = a_{0y} + \frac{p}{a_{1y} + a_{2y}p}$$

$$Y_m = \Delta\sigma_m = a_{0m} + \frac{p}{a_{1m} + a_{2m}p}$$

$$Y_r = \Delta r = a_{0f} + \frac{p}{a_{1f} + a_{2f}p} \qquad (4\text{-}5)$$

where

Y_y, Y_m, Y_r = yield, limit, and residual surfaces,

a_k = parameters defining strength surfaces (a_{0f} for concrete = 0), and

p = hydrostatic pressure which is one-third of the total stress.

The general yield criterion for the K&C concrete model is given by:

$$f = J_2 - \left[F_f(I_1, \theta)\right]^2 = 0 \qquad (4\text{-}6)$$

where

J_2, I_1, θ = the stress invariants, and

F_f = the shear failure surface.

It should be noted that the yield criterion has a similar form to the CSCM yield criterion but with fewer terms. Unlike the CSCM model, the K&C model does not account for the effect of porosity on the shear strength deviatoric stress. In short, the K&C model employs a yield surface without the hardening cap (see figure 4.2).

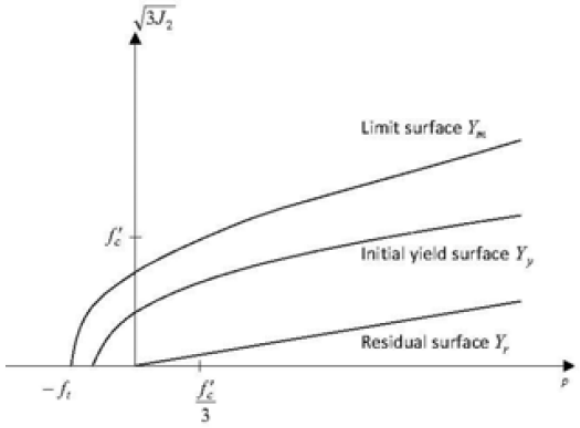

Figure 4.2 K&C meridian profiles *(Brannon and Leelavanichkul 2009)*

In order to reshape the yield surface from a circle to a cylindrical Lode coordinate, the Willam-Warnke Lode angle function (Willam 1975) was provided (figure 4.3).

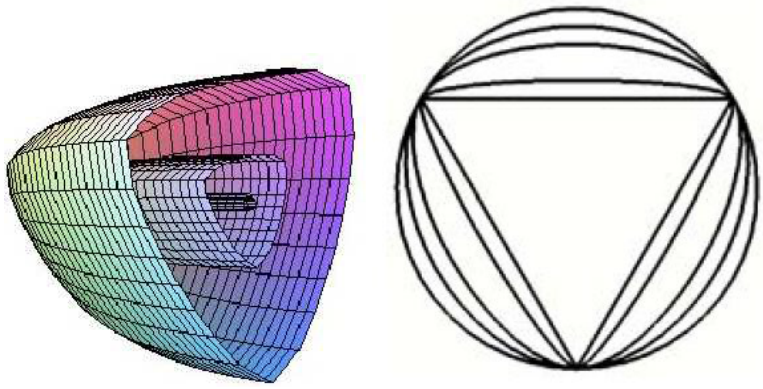

Figure 4.3 Different views of K&C yield surface:3D stress space and Deviatoric section *(Brannon and Leelavanichkul 2009)*

Prior to reach the yield surface, Hooke's law is used for the elastic behavior of the material. The isotropic behavior is governed by a compaction curve or equation of state (EOS). The EOS prescribes a set of pressures, unloading bulk moduli, and volumetric strains. The model scales the bulk moduli entered as part of EOS by the factor φ, as follows:

$$\varphi = \frac{-\Delta\varepsilon}{-\Delta\varepsilon + \left(p - p_f\right)/K_U} \tag{4-7}$$

where

$\Delta\varepsilon$ = $\varepsilon_{v,min}$ - ε_v,

ε_v = volumetric strain, and

K_U = unload/reload bulk modulus from the EOS.

The K&C model considers the porosity effect in the compaction EOS.

4.2.2 Implementation in LS-DYNA

The last version of the K&C concrete model in LS-DYNA is model type 72 release III (MAT_CONCRETE_DAMAGE_REL3). In this update, an automatic model parameter generation based on the unconfined compressive strength and the maximum aggregate size was added. Seven cards are expected for this model and an EOS is also required for the pressure-volume strain response. However, using only the unconfined compressive strength (as well as mass density and Poisson's ratio), the model can generate other parameters. The strain rate effect can be taken into account by introducing a load curve (LCRATE).

4.3 Solid Elements Formulations

Solid bodies can be formulated using three-dimensional solid elements. Solid elements can represent the entire structure where no geometric assumptions are required, and the boundary conditions are more realistic (Erhart 2011). However, using the solid bodies will increase the CPU time and post-processing efforts. Several solid elements formulations are implemented in LS-DYNA via the ELFORM variable in the SECTION_SOLID card, which allows the user to select the desired formulation. In this study, fully integrated (ELFORM = 2, -1, -2) and under-integrated (ELFORM = 1: default) hexahedra solid elements were selected for modeling the concrete material. New fully integrated solid elements (ELFORM = -1 & -2) are identical to the ordinary one (ELFORM = 2) but with enhanced strain formulation, which was done by modifying the Jacobian matrix (Erhart 2011). A summary of their properties adopted from (Erhart 2011) is presented below:

Table 4.1 Hexahedra elements in LS-DYNA - modified from *(Erhart 2011)*

	Under-integrated	Fully integrated		
		Regular formulation	Efficient formulation	Accurate formulation
ELFRM	1	2	-1	-2
Characteristics	under-integrated constant stress	too stiff, worse in poor aspect ratios, shear locking	enhanced strain formulation compared to regular formulation, effective for shear locking	enhanced strain formulation compared to regular formulation, effective for shear locking
Application	efficient in large deformations	more unstable in large deformations	more unstable in large deformations	more unstable in large deformations
Hourglass	usually needs hourglass stabilization	no hourglass stabilization	hourglass tendencies	hourglass tendencies
Computational Cost	usually faster than fully integrated elements	slower than type 1	approximately 1.2 times the type 2	approximately 4 times the type 2

Chapter 5 Single Element Simulation

A single element simulation was conducted to investigate the CSCM and K&C concrete models under tension and compression at various loading rates and input variables. This simulation was performed under unconfined uniaxial tension and compression in which the loading is applied as a displacement-controlled movement of the top four nodes of the element.

5.1 Continuous Surface Cap Model

5.1.1 Effect of Loading Rate

The effect of loading rate on the behavior of the CSCM material model was evaluated by simulating a single element model under compression. It was assumed that the element represents a concrete block with a compressive strength of 40 MPa and a maximum aggregate size of 9.5 mm. The simulations were performed at two different rates: 10-2 ms-1 and 10-8 ms-1. The higher loading rate represents impact loading while the lower loading rate represents quasi-static loading. Additionally, the compatibility of the CSCM model with explicit and implicit solvers was evaluated. The models with higher loading rates were simulated using the explicit solver while the models with lower loading rates were simulated using the implicit solver. The implicit solver allows larger time steps as compared to explicit time discretization. Hence, the implicit solver is suitable for simulation of quasi-static tests where the test duration is relatively long.

The CSCM model allows either to consider or disregard the strain rate effect using IRATE parameter. Additionally, in implicit simulations there is an IRATE parameter on CONTROL_IMPLICIT_DYNAMICS keyword that needs to be changed according to the simulation condition. The sensitivity of the CSCM model to strain rate values was investigated for each loading case.

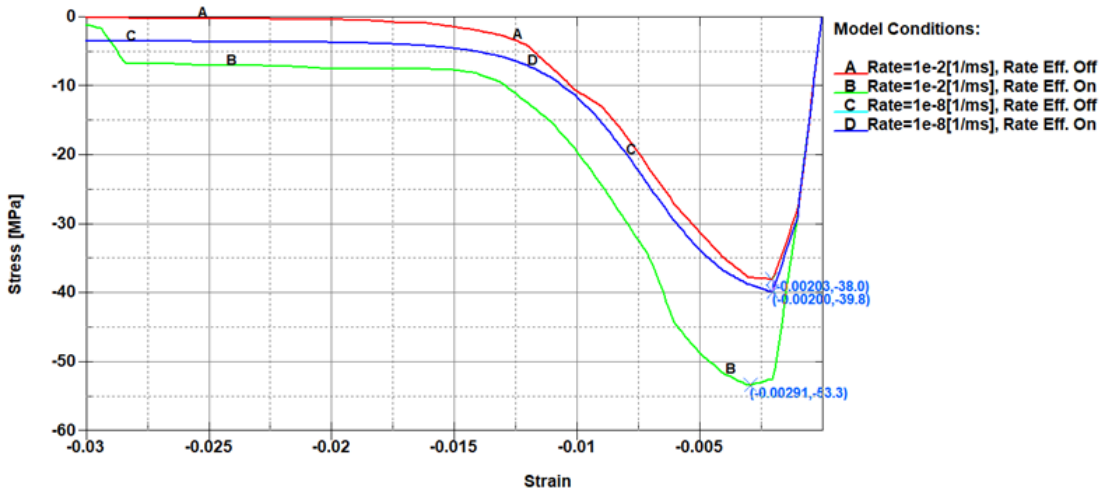

Figure 5.1 Effect of loading rate on strain-stress behavior of an unconfined single element under compression

Table 5.1 Results of unconfined single element simulation under uniaxial compression for a concrete material with $f_c^{'}$ equal to 40 MPa and D_{max} equal to 9.5 mm.

Loading rate [1/ms]	Strain rate effect	Elastic modulus [GPa]	Strain at damage initiation	Strength [MPa]
1.0e-2	Off	19.0	-0.002	38.0
1.0e-2	On	19.5	-0.002	53.3
1.0e-8	Off	19.5	-0.002	39.8
1.0e-8	On	19.5	-0.002	39.8

The stress-strain relationship of the unconfined single element model under compression is plotted in figure 5.1. Also, important values such as elastic modulus and strength were

extracted from the simulation and are summarized in table 5.1. The following observations were made based on the results shown in figure 5.1:

- The CSCM model is a rate-dependent model since the strength of the material increases with an increasing rate. Such behavior is in agreement with published experimental results (Grote, Park, and Zhou 2001). The loading rate effect can be significant, depending on the input (i.e., compressive strength). As shown in figure 5.1, a change in the loading rate from 10-8 ms-1 to 10-2 ms-1 increased the maximum strength up to 30%.
- Models with a slow loading rate (10-8 ms-1) result in a maximum strength close to the input maximum strength (f_c^'). Models with a fast loading rate (10-2 ms-1) yield a similar maximum strength when the loading rate is set to Off.
- The loading rate effect (IRATE) does not change the response of the CSCM model at low loading rates.
- For implicit models, the damage of the element becomes saturated at a small value (5% of maximum strength) but did not reach zero.
- The loading rate did not show a substantial effect on the elastic modulus in the CSCM concrete model.

5.1.2 Effect of the Eroding Parameter

As mentioned earlier, the CSCM model is advanced by using the element erosion methodology when it is implemented into LS-DYNA software. Erosion of an element is controlled by the parameter ERODE on the MAT_CSCM keyword. In the MAT_CSCM model, elements erode when damage exceeds 0.99 and the maximum principal strain exceeds 1-ERODE. If ERODE is equal to 1.0, erosion is based merely on the damage and is independent of strain level (Murray 2004; Hallquist 2013)

The effect of the ERODE parameter on element erosion is discussed in this section. Simulations were conducted at two loading rates: 10^{-2} ms^{-1} and 10^{-8} ms^{-1}. The amount of accumulated damage of the element with respect to the maximum principle strain is plotted in figure 5.2. The following conclusions were made based on the results of single element simulation:

- In the explicit simulation, the amount of damage to the element accumulates to 1 when the loading increases. Thus, the element is eroded when the damage reaches a value beyond 0.99 and the maximum principal strain reaches 1-ERODE.
- The elements that were simulated using implicit solver did not erode even when maximum principle strain passed the limit value (1-ERODE). This is due to the amount of damage to the element saturated to a value less than 0.99.

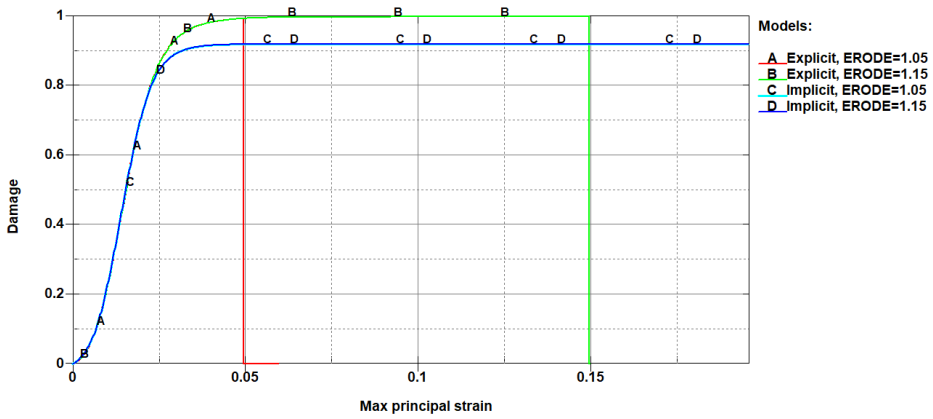

Figure 5.2 Effect of the ERODE parameter on the erosion behavior of unconfined single element under compression loading

5.1.3 Effect of the Input Values of the CSCM Model

A single element simulation was conducted to evaluate the sensitivity of the MAT_CSCM_CONCRETE model to its input parameters. Both the unconfined compressive strength and the maximum aggregate size are varied to investigate the effect of the input values on the behavior of the CSCM_CONCRETE model. The simulations were conducted using an explicit solver. To exclude the effect of loading rate, the model was run with the strain rate effect set to *Off*. The stress-strain relation of the unconfined single element model under compression and tension are plotted in figure 5.3 and figure 5.4, respectively. The following observations were made based on the results of the single element simulation:

- The compressive strength values generated by the CSCM model are slightly different than the compressive strength provided as input values (f_c').
- Maximum aggregate size only affects post-peak behavior and is directly related to dissipated energy; as the maximum aggregate size increases, the amount of dissipated energy also increases.
- The tensile strengths calculated by the CSCM model are less than 10% of the compressive strength.

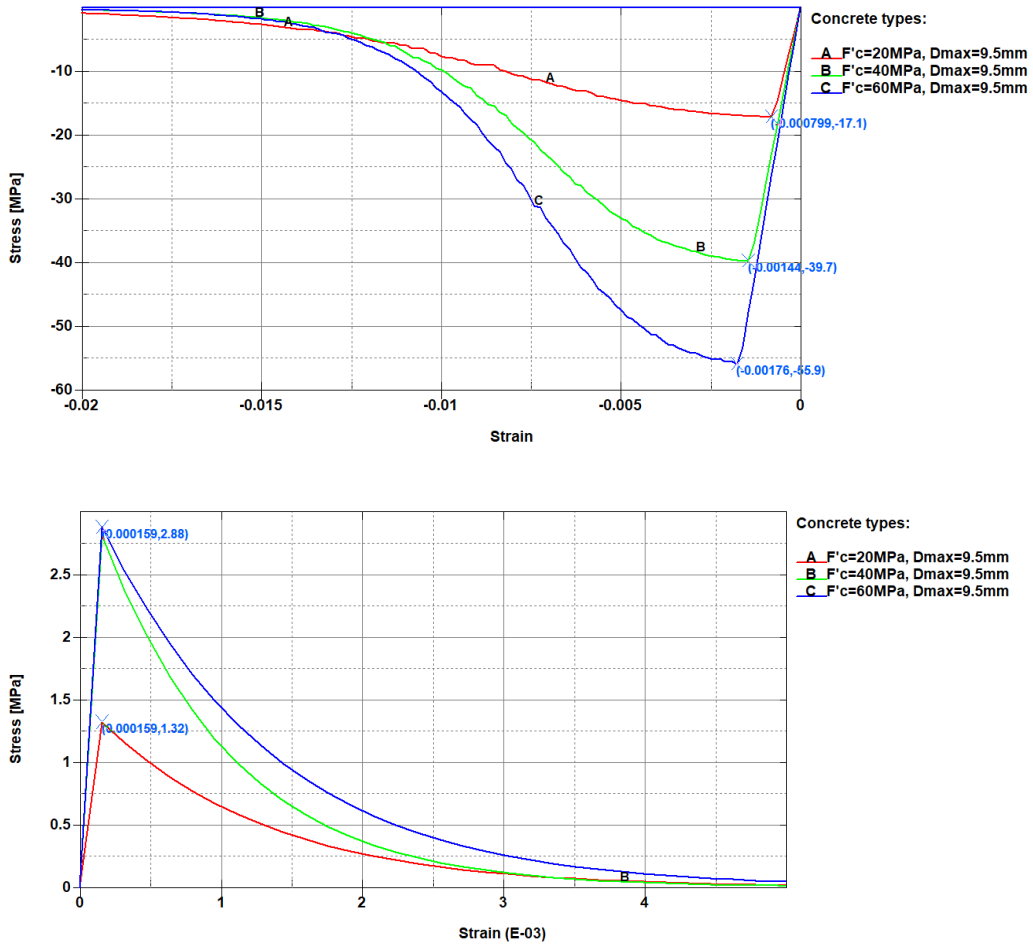

Figure 5.3 Effect of compressive strength on strain-stress behavior of an unconfined single element under compression (top) and tension (bottom) loading-CSCM model

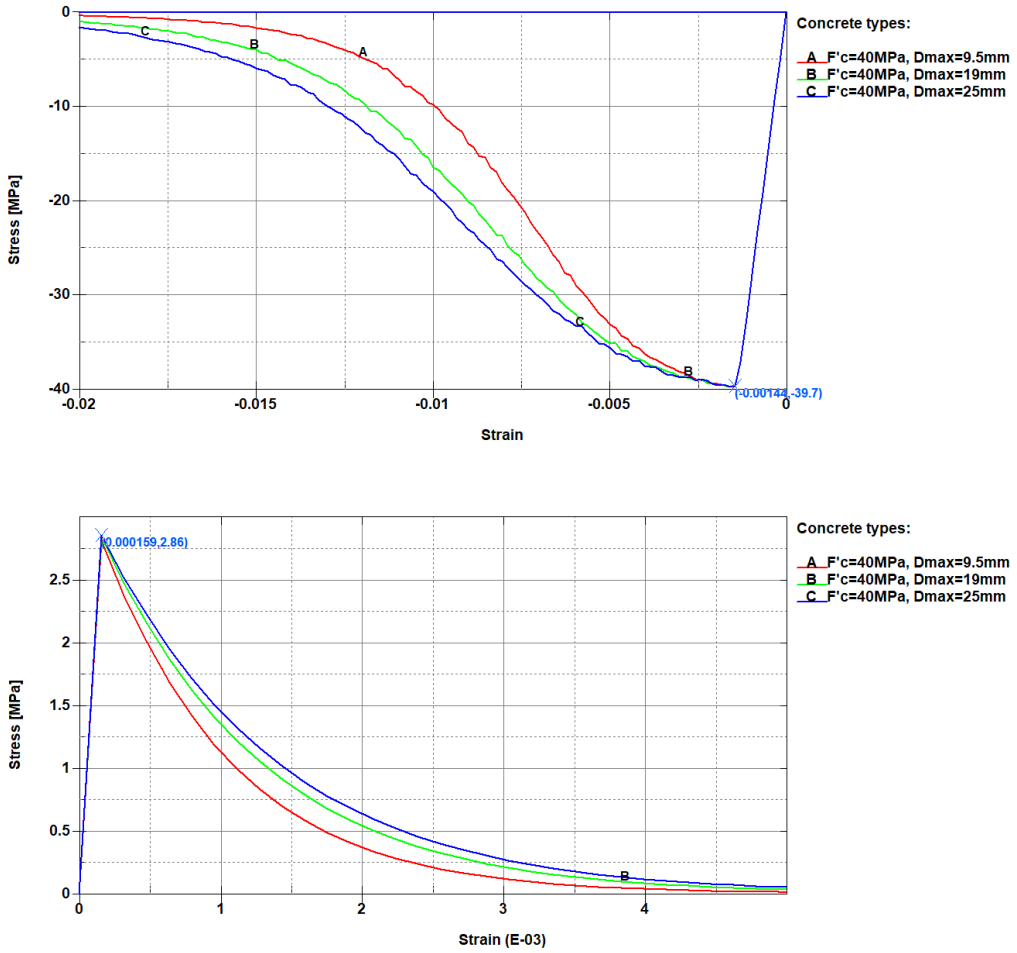

Figure 5.4 Effect of maximum aggregate size on strain-stress behavior of an unconfined single element under compression (top) and tension (bottom) loading-CSCM model

5.2 Karagozian & Case (K&C) Concrete Model

5.2.1 Effect of the Input Values of the K&C Model

Unlike the CSCM material model, the effects of parameters such as erosion or modulus recovery are not adjustable in the K&C model. Therefore, only the effects of input values (i.e., compressive strength and maximum aggregate size) are discussed in this section. Simulations were conducted using an explicit solver. Stress-strain curves of the unconfined single element model under compression and tension are presented in figure 5.5 and figure 5.6, respectively.

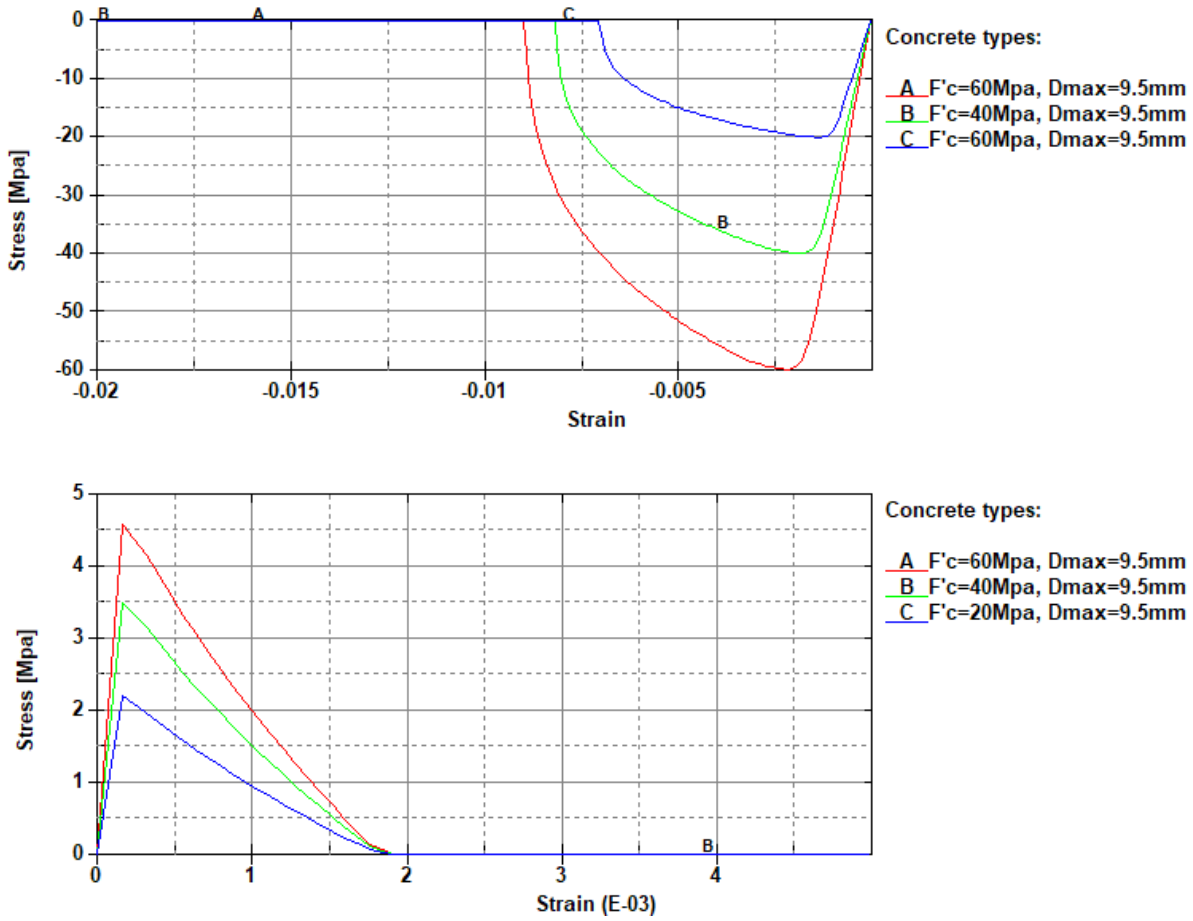

Figure 5.5 Effect of compressive strength on the strain-stress behavior of an unconfined single element under compression (top) and tension (bottom) loading- K&C model.

According to figure 5.5, the peak compressive strength values generated by the K&C model correspond accurately to the exact values of the input compressive strength. A disagreement between the CSCM model (fig. 5.3) and the K&C model was observed, which indicated that the K&C model more accurately determined a single element stress value. Moreover, in tension, the peak stress values followed a reasonable path. The overall shape of the stress-strain curve in the K&C and CSCM models is different after passing the peak stress. The

K&C model exhibited brittle behavior while the CSCM model exhibited a strain-softening behavior.

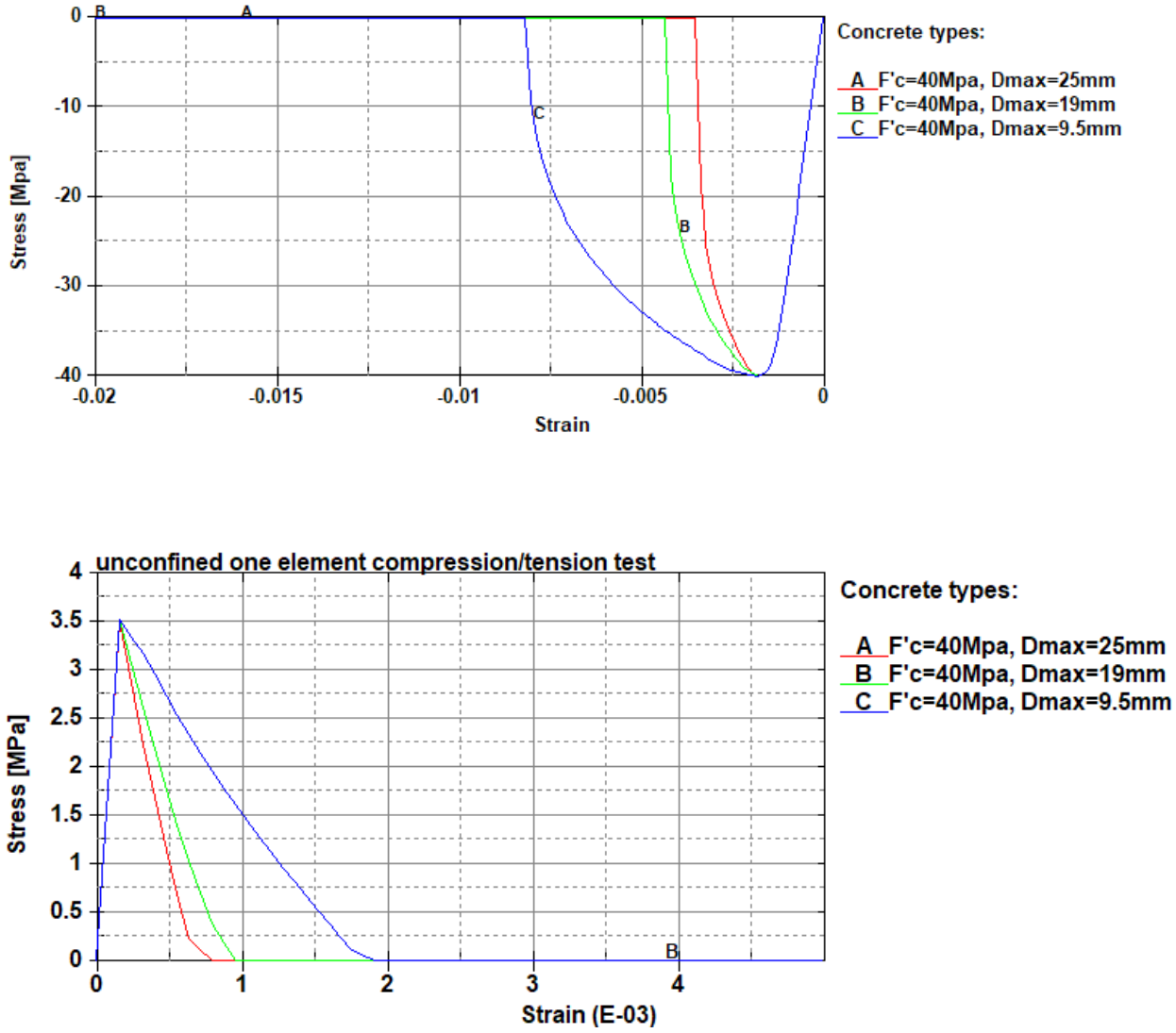

Figure 5.6 Effect of maximum aggregate size on strain-stress behavior of an unconfined single element under compression (top) and tension (bottom) loading- K&C model

Maximum aggregate size is an optional input in the K&C model and does not have any effect on the maximum stress value for both compression and tension cases. Similar to the

CSCM model (fig. 5.4), the only difference is in the post-peak behavior in which the bigger aggregate size selection resulted in higher energy dissipation. However, the effect of aggregate size is more significant in the K&C model.

Chapter 6 Simulation of Quasi-Static Tests

Two quasi-static tests of concrete samples, including uniaxial compression and four-point bending tests, were simulated in LS-DYNA using the two models: K&C and CSCM. Inputs for both models were generated by an automated model input generator in which only compressive strength and maximum aggregate size were required. The compressive strength of the concrete material used in this chapter is 62.5 MPa (9 ksi) and its maximum aggregate size is 10 mm (0.39 inch). The values of the other model parameters (e.g., ERODE and RECOV) and the coefficient of friction at the contact surface were determined by a trial and error procedure that was performed until a satisfactory agreement between simulations and experiments was achieved.

6.1 Uniaxial Compression Test

Numerical simulation of the uniaxial compression test (Winkelbauer et al. 2016) is presented in this section. Additionally, to assess the viability of the model, failure mechanisms are analyzed, and the results of the simulation are compared with the experimental results.

6.1.1 Description of the Model

Uniaxial compression test settings and the corresponding finite element model are presented in figure 6.1. A cylindrical sample with a diameter of 4 inches and a height of 8 inches is placed between two steel plates. The top plate moves downward at a constant rate of 0.0127 mm/sec while the bottom plate is fixed. The steel bearing plates are modeled as rigid bodies using MAT_RIGID keyword. Contact between the concrete cylinder and bearing plates is defined using CONTACT_SURFACE_TO_SURFACE keyword. Frictional resistance between the loading plate and the concrete cylinder has a direct effect on the softening behavior of the material (Shah et al. 2000). In the results shown in figure 6.2, 0.30 was selected as the static and dynamic coefficient of friction in the CONTACT card. In order to find the mesh size sensitivity,

an optimization study was conducted to find the element size which achieves sufficient accuracy and requires reasonable computation time. As a result, element sizes were selected within 5-8 mm for the cylinder.

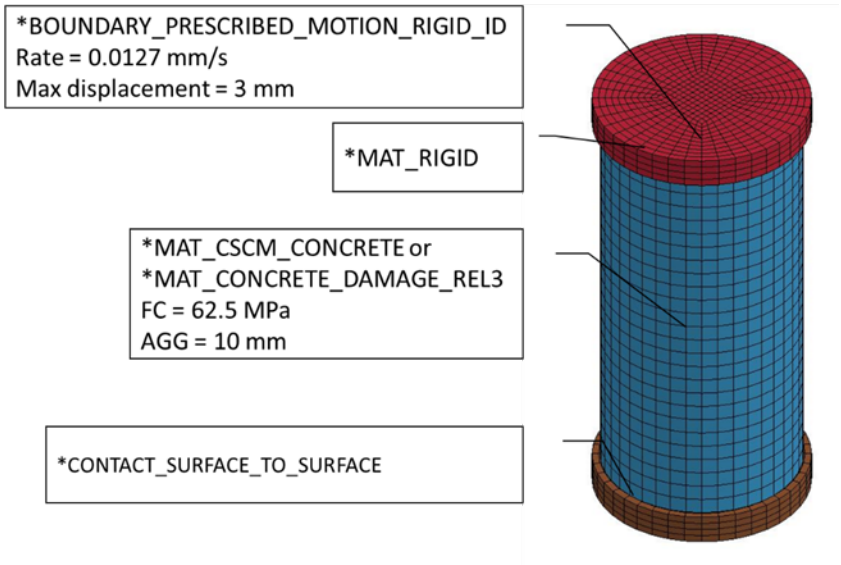

Figure 6.1 The LS-DYNA model of the uniaxial compression test

6.1.2 Simulation Results

The uniaxial compression model was validated by comparing the results of the simulation with the experimental results. The failure mode and stress-strain curve of the actuator were selected for comparison. As can be seen in figure 6.2, in the uniaxial compression test, both the CSCM and K&C models accurately predicted the experimental results until the failure point was reached. However, numerical solvers and element formulations were selected differently. For the CSCM model, the best validation results were generated with implicit solver and selection of fully integrated solid elements (ELFORM = -1), while for the K&C model, the best validation results were generated with explicit solver and constant stress solid element (ELFORM = 1).

Post-failure behavior was different between the CSCM and K&C models. The CSCM model exhibited more of a ductile behavior while the K&C displayed more brittle behavior. Concrete post-failure behavior was dependent on concrete strength (see fig. 6.3), where higher levels of strength resulted in more brittle behavior. In this study, concrete with a compressive strength of 62.5 MPa was employed. This level of compressive strength indicates that the concrete is of relatively high strength; thus, brittle behavior is expected. To further calibrate the CSCM model, contact with an extremely low coefficient of friction (0.03) was examined, but the stress-strain curve was not significantly different (fig. 6.4).

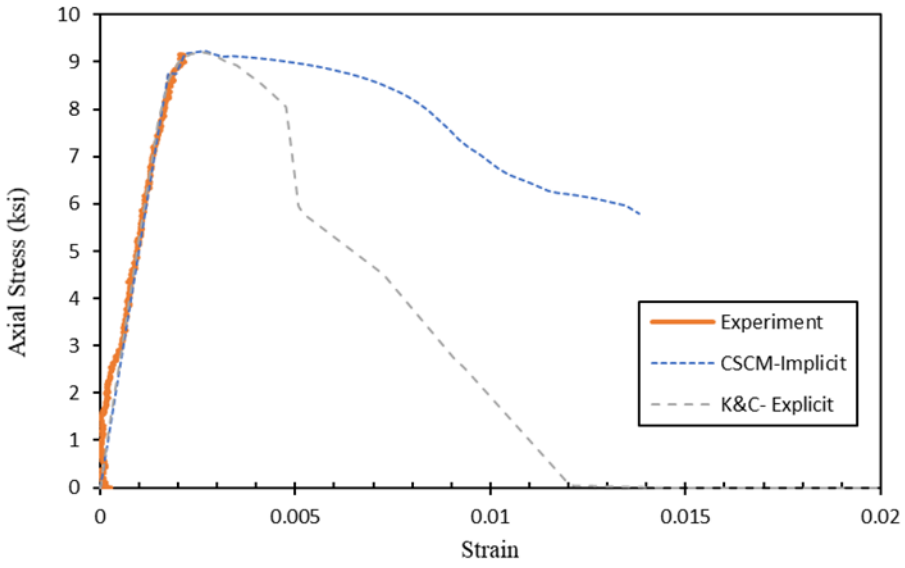

Figure 6.2 Axial stress-axial strain curve of uniaxial compression test - validation of simulation with experiments

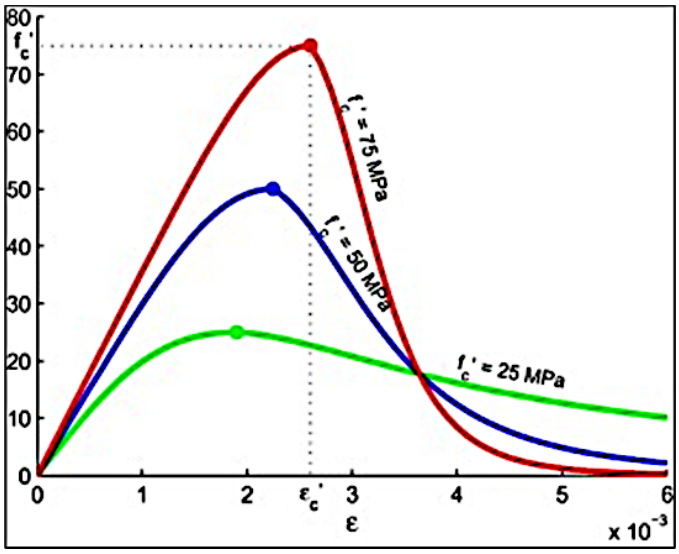

Figure 6.3 Stress-strain curves of the uniaxial compression test (Collins 1993).

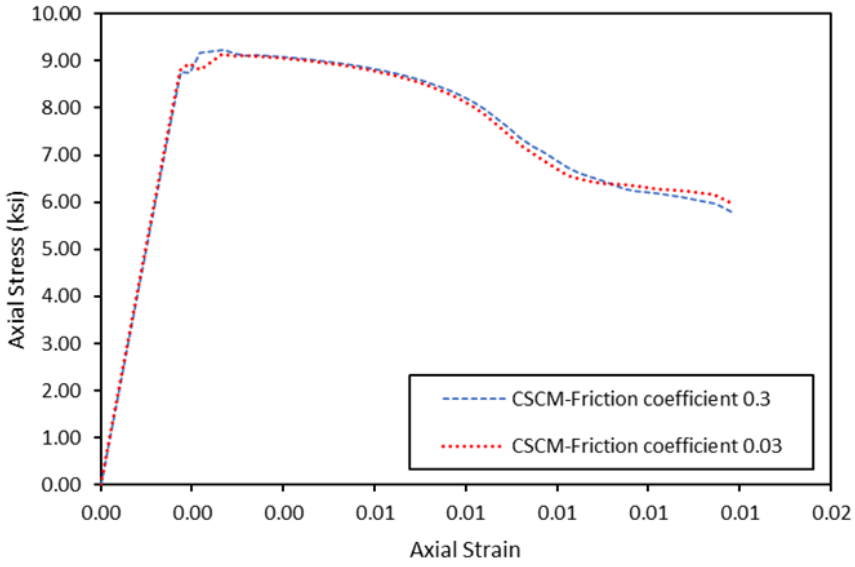

Figure 6.4 Effect of contact friction on the compression test with the CSCM concrete model.

The effect of numerical solvers (i.e., explicit and implicit) can be found from figure 6.5 and figure 6.6. It is clear that the difference was more noticeable in the K&C concrete model.

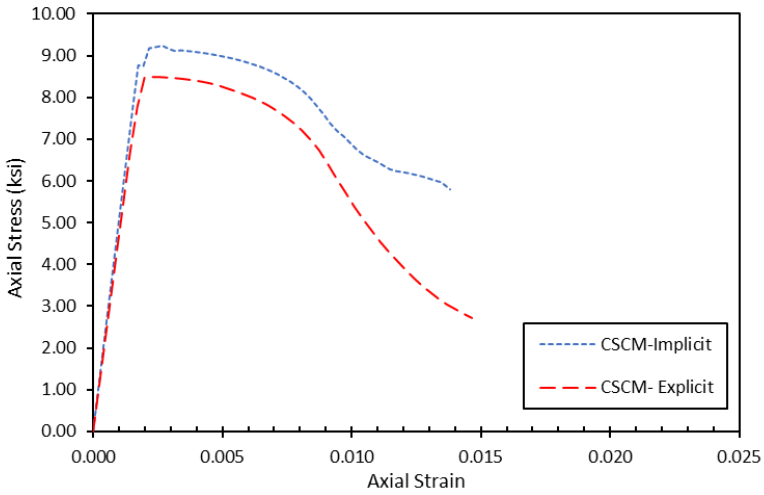

Figure 6.5 Axial stress-axial strain curve of the uniaxial compression test: Comparison of implicit vs. explicit solvers using the CSCM concrete model.

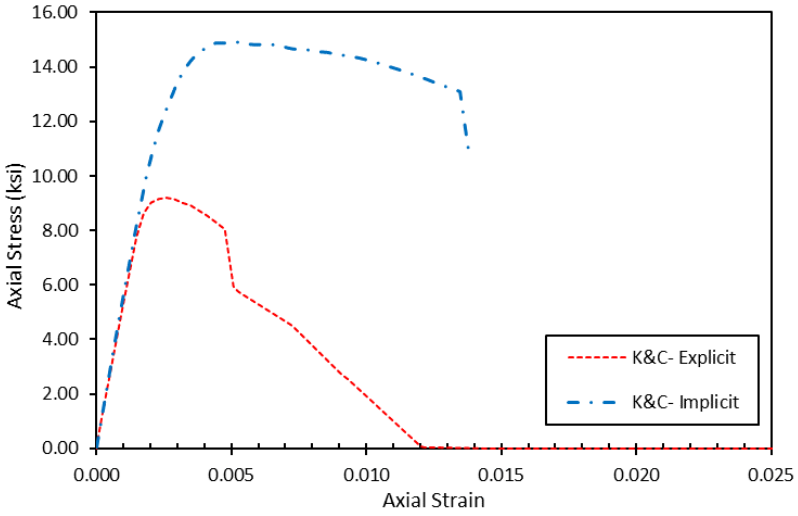

Figure 6.6 Axial stress-axial strain curve of the uniaxial compression test: Comparison of implicit vs. explicit solvers using the K&C concrete model.

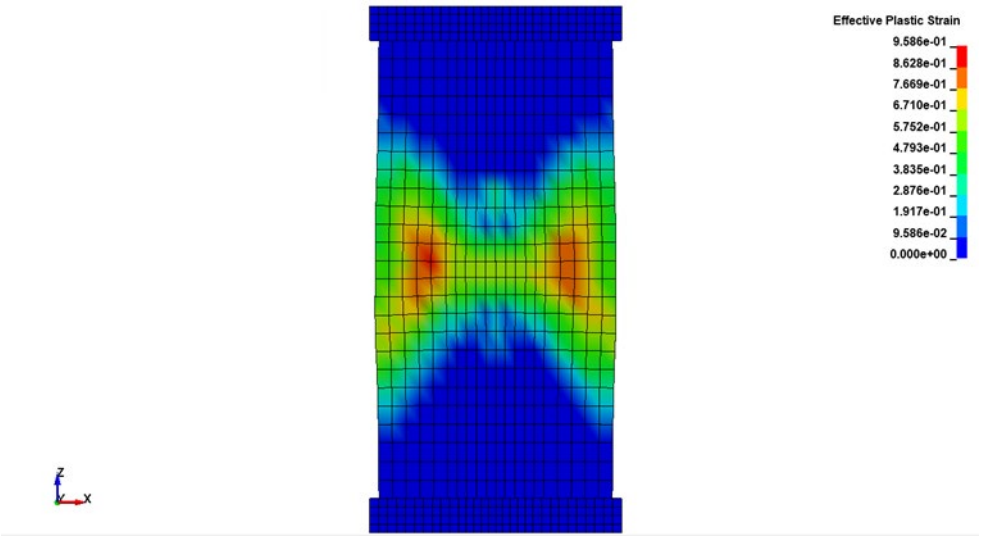

Figure 6.7 Damage zone contours in the uniaxial compression test-CSCM concrete model.

The failure mode of the cylinder samples in the compressive testing depends on the friction condition of the two ends of the specimen. The damage zone contours in the CSCM model are presented in figure 6.7. The damage zone contours agree with the typical failure mechanism of concrete specimens under compression. The cone-shaped failure surface could imply that the friction between the concrete sample and plates is relatively high. The friction at the loading plates restrains lateral expansion of the concrete cylinder and results in two relatively undamaged cones when the concrete cylinder fails.

6.2 Four-point Bending Test

Numerical simulation of the four-point bending test (Winkelbauer et al. 2016) is presented in this section. The simulation was conducted for two different support span lengths, which captured either flexural or shear failure modes. Viability of the model was evaluated by comparing the simulation results with experimental results. Similarly, the CSCM and K&C concrete models were compared.

6.2.1 Model Description

The four-point bending finite element model is presented in figure 6.8. The beam cross-section is 6 inches × 6 inches and the length is 22 inches. The test was simulated with support spans of 18 inches and 9 inches where the failure modes were expected to be flexural and shear, respectively. The top actuators moved downward with a constant rate of 0.0075 mm/sec (0.0003 inch/sec) while the bottom supports were fixed. The steel supports and the loading pins were modeled as rigid bodies using MAT_RIGID keyword. Contact between the concrete beam and steel parts was defined using CONTACT_SURFACE_TO_SURFACE keyword. Fine mesh sizes were selected in the beam (around 7-8 mm). Also, 0.10 was selected as the static and dynamic coefficient of friction in the CONTACT card.

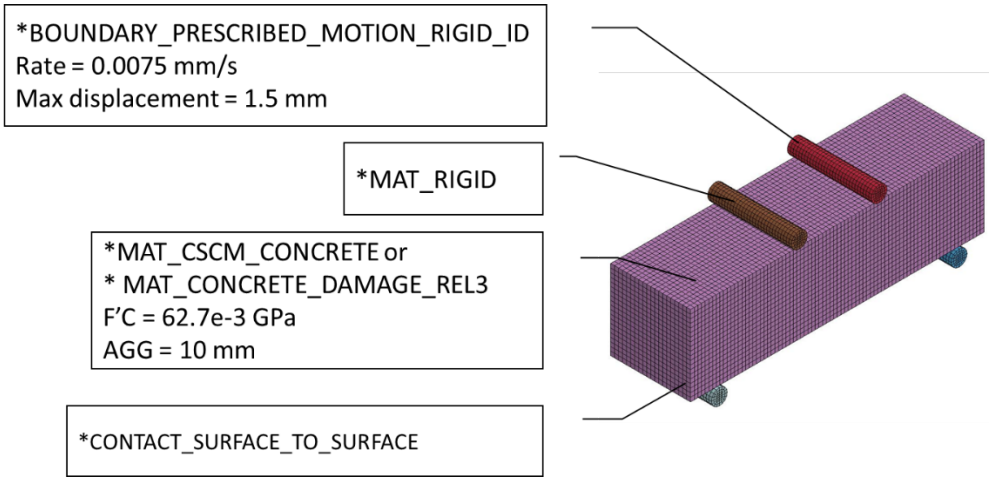

Figure 6.8 LS-DYNA model of the four-point bending test.

6.2.2 Simulation Results

The force-time curve of support spans of 18 inches and 9 inches are plotted in figure 6.9 and figure 6.10, respectively. The support span of 18 inches (span-to-depth ratio of 3.0) accounted for the flexural behavior of concrete. Both CSCM and K&C models were

approximately validated by the experimental test results, although different numerical solvers were selected. The experiment peak load was 5.9 kips, which resulted in a flexural fracture pattern (fig. 3.3). The support span of 9 inches (span-to-depth ratio of 1.5) accounted for the shear behavior of concrete. The peak force of 39.77 kips was not simulated by either of the models. For the CSCM model, different model parameters were tested (such as erosion or modulus recovery) but they did not show any dramatic changes. For shear strength, both models failed sooner than the testing.

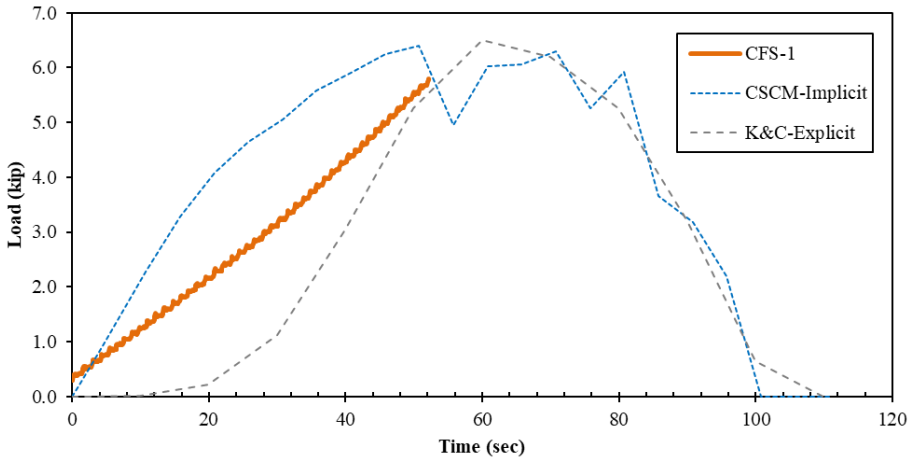

Figure 6.9 Force-time plot of the four-point bending test for a span-to-depth ratio of 3.0

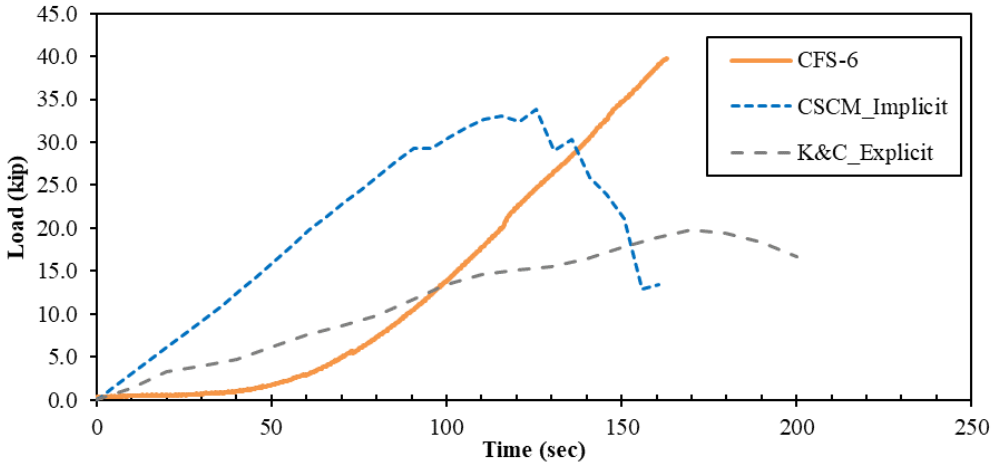

Figure 6.10 Force-time plot of the four-point bending test for a span-to-depth ratio of 1.5

Damage contours in the CSCM model for both span ratios are shown in figure 6.11 and figure 6.12. The effect of element erosion is visible in flexural failure. In comparison with the experimental tests, the failure pattern took place in similar zones. As expected, the elements with the highest plastic strain are close to support spans in shear failure, while they were at around mid-span for flexural failure.

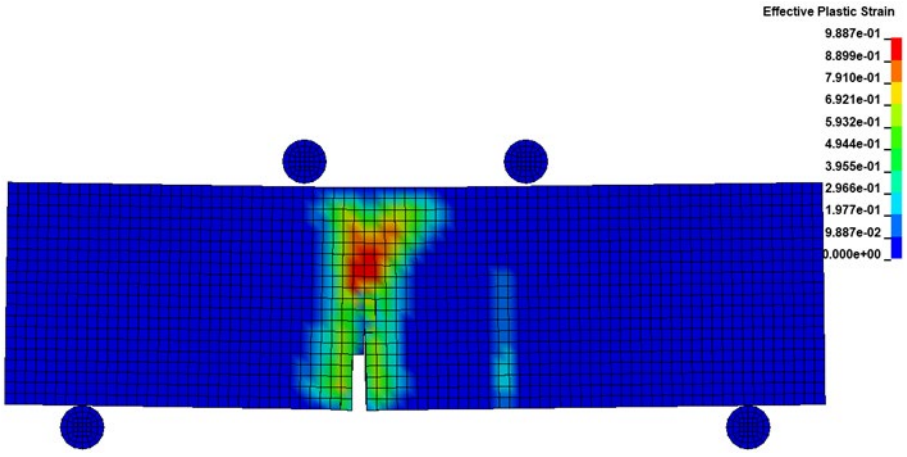

Figure 6.11 Damage contours of the bending test for a span-to-depth ratio of 3.0 - CSCM model.

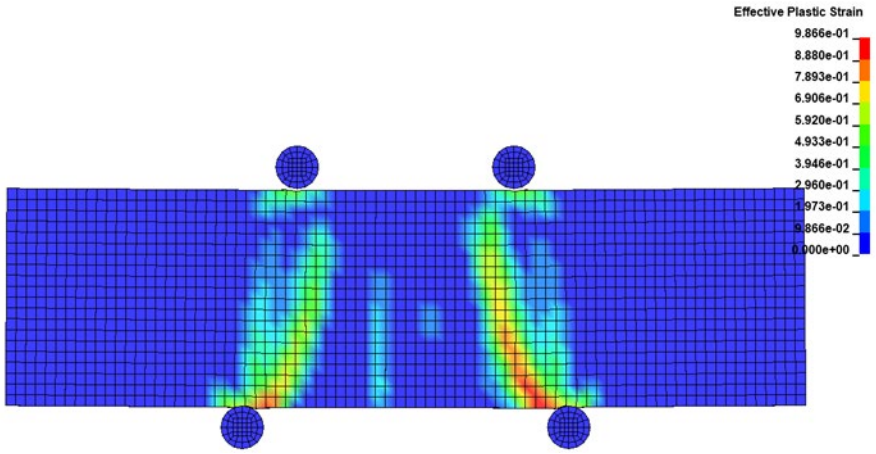

Figure 6.12 Damage contours of the bending test for a span-to-depth ratio of 1.5 - CSCM Model.

Damage contours in the K&C model for both span ratios are shown in figure 6.13 and figure 6.14. For the 18 inches span, the K&C model predicted a vertical fracture around the mid-span. However, for the 9 inches span, the damage zones were developed in a wider area within the spans.

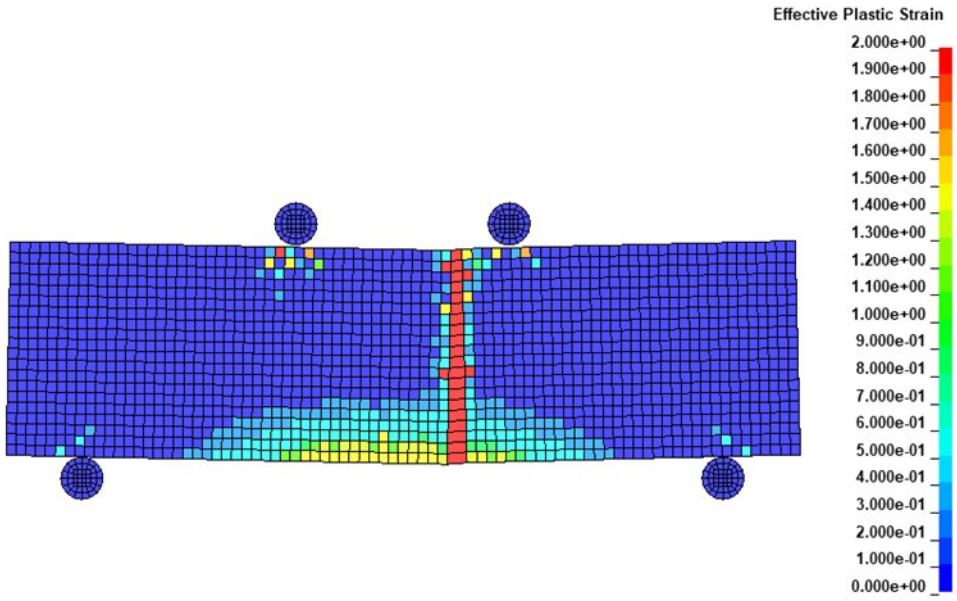

Figure 6.13 Damage contours of the bending test for a span-to-depth ratio of 3.0 - K&C model.

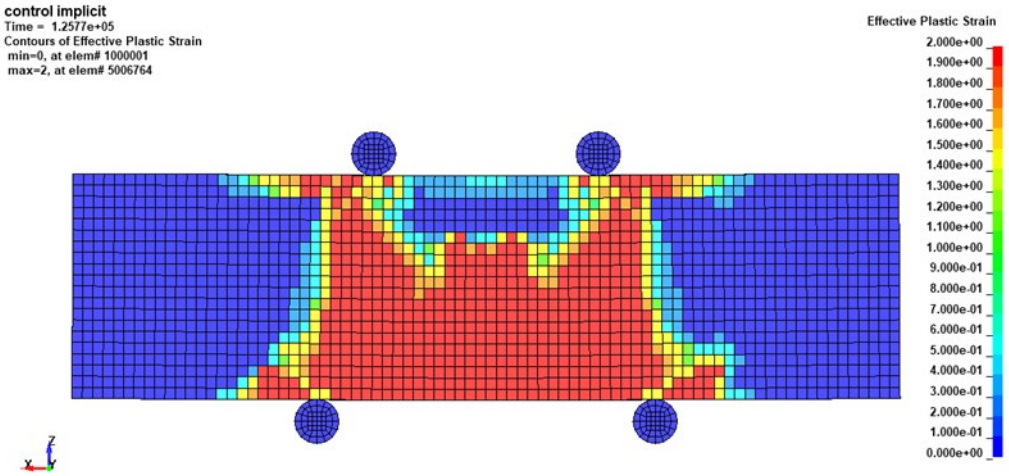

Figure 6.14 Damage contours of the bending test for a span-to-depth ratio of 1.5 - K&C model.

6.2.3 Summary

In this chapter, three different types of concrete failure (i.e., compression, shear, bending) were tested in order to evaluate the performance of the CSCM and K&C concrete models. Both models successfully predicted the behavior of concrete in compression. Moreover, the simulation results in the flexural test were close enough to the experiments. In shear, the predicted peak force was not as accurate as flexural and compression. However, the calculated shear stress over the beam cross-section showed that the difference was not huge. A summary of the comparison between experimental tests and model simulation results is provided in table 6.1.

Table 6.1 *Summary of experimental tests with simulation results- quasi-static tests*

Property	Test Results	CSCM Model	K&C Model
Peak Value (Compression), MPa	63.15	62.65	63.40
Peak Value (Bending), MPa	1.11	1.20	1.17
Peak Value (Shear), MPa	7.62	6.70	3.65

Chapter 7 Simulation of Impact Tests

In this chapter, the behavior of the CSCM and K&C concrete models was evaluated by simulating low-velocity impact to plain concrete beam specimens with a drop weight. The simulation results were compared with similar low-velocity impact test results taken from other studies (Yilmaz et al. 2014; Memon et al. 2019), which was discussed in Chapter 3.

7.1 Model Description

The discretized model of the drop weight test is shown in figure 7.1, which includes the concrete beam with dimensions of 150 mm × 150 mm × 710 mm, rigid concrete supports with dimensions of 150 mm × 150 mm × 150 mm, the steel plate with dimensions of 150 mm × 50 mm × 20 mm, and the steel impactor with a weight of 5.25 kg. Further details regarding the employed concrete and steel properties are shown in table 7.1 and table 7.2. In order to reduce computational time, instead of assigning a drop height of 300 mm (employed in the actual test), the energy conservation equation was used to calculate an equivalent initial velocity of 2.42 m/sec. Regarding the contact model, two models were employed:

CONTACT_SURFACE_TO_SURFACE was generally defined with static and dynamic friction coefficients of 0.01 at the steel-steel surfaces and 0.08 at the concrete-concrete surfaces. A SOFT parameter of 2 was also assigned to the contact model.

CONTACT_AUTOMATIC_SURFACE_TO_SURFACE_TIEBREAK was defined to connect the two sections of the impactor as well as tying the steel plate to the concrete beam. This type of connection is well-suited for transmitting compressive and tensile stresses (Memon et al. 2019). Here, the SOFT parameter of 1 was allocated. Constant stress hexahedra solid elements (ELFORM = 1) with element size of 5 mm were employed in the beam which was selected based on the element size study optimization.

Table 7.1 Concrete properties used in the FEM model for the drop weight test

Property	Value
Density	2400 Kg/m^3
Compressive Strength	24.6 MPa
Maximum Aggregate Size	15 mm
Poisson's Ratio	0.19

Table 7.2 Steel properties used in the FEM model for the drop weight test

Property	Value
Density	7580 Kg/m^3
Elastic Modulus	200 Gpa
Poisson's Ratio	0.30

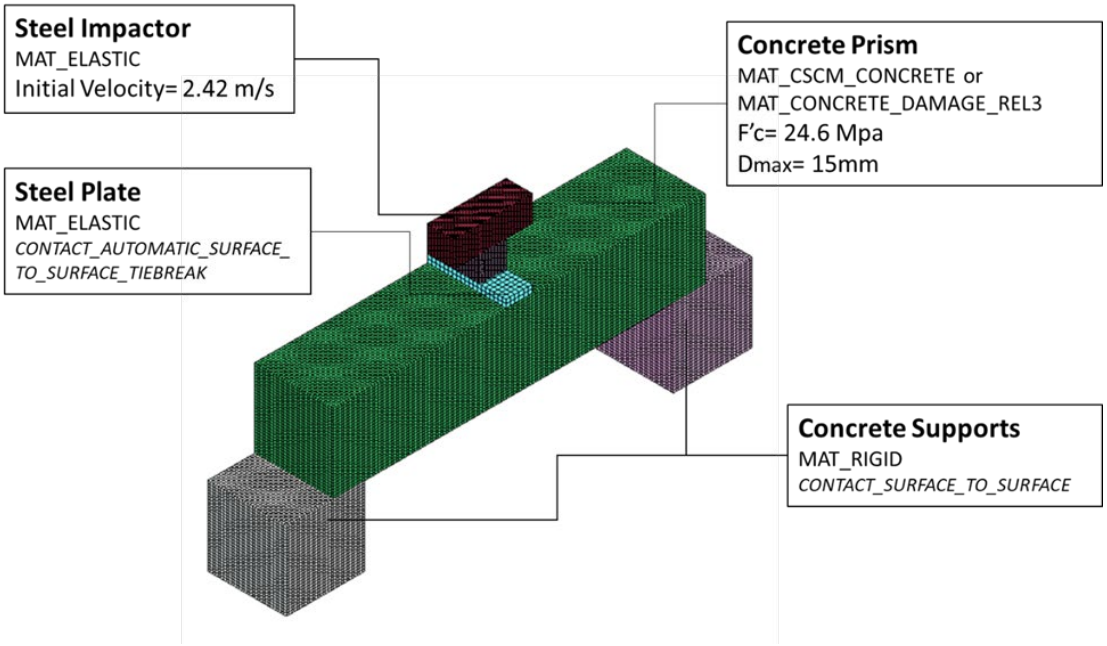

Figure 7.1 The LS-DYNA model of the drop weight test

7.2 Simulation Results

Similar to the experimental study (Yilmaz et al. 2014), the node on the top surface of the beam at a distance of 150 mm (along the length) from the center was selected in order to obtain acceleration and displacement values (stored in NODOUT). The force value was also obtained from the reaction force at the supports (stored in RCFORC). The force-displacement curve for both models is shown in figure 7.2, which shows that the peak impact load was different in the CSCM and K&C models. The peak load from the experiment was 13.1 kN at a corresponding displacement of 0.1730 mm, which was better predicted by the CSCM model.

An acceleration curve usually provides useful information in any impact test. The acceleration-time graph is shown in figure 7.3, which shows that the acceleration in the K&C model experienced a slightly higher resonance rather than in the CSCM model; however, both models displayed similar overall behavior. The experimental study showed that the maximum

positive and negative acceleration was 2,555 and -2,677 m/sec^2, respectively, which is in better agreement with the results predicted by the CSCM model.

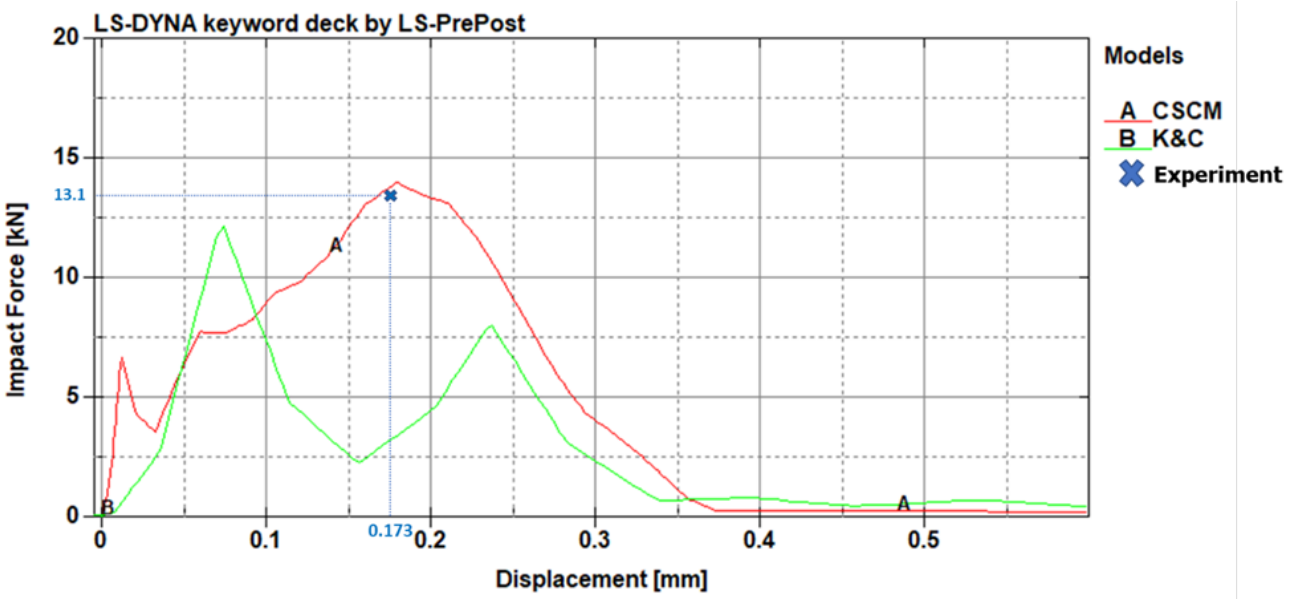

Figure 7.2 Impact force versus deflection curve comparing CSCM and K&C models with the experimental study- drop weight test.

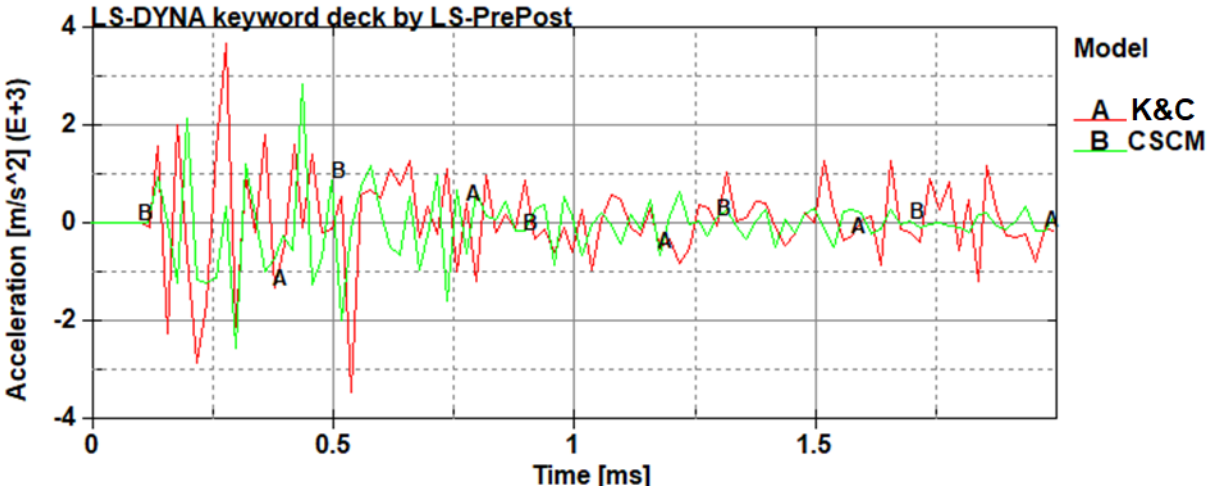

Figure 7.3 Acceleration versus time plot comparing CSCM and K&C models- drop weight test.

The damage contours at the time of 2 ms predicted by the CSCM and K&C models are shown in figure 7.4 and figure 7.5, respectively. As previously mentioned, the CSCM model has the capability of element erosion, which is clearly displayed in figure 7.4. The CSCM model showed more localized damaged zones right beneath the impact location, while the K&C model predicted the damage zones in a more scattered manner in the whole concrete beam with narrower widths where the tensile capacity of concrete was insufficient. Based on a comparison of the damage contours generated by the models with the experimental result (fig. 7.6), the CSCM model prediction seems closer to reality, as the experimental results also showed the main crack at the center of the beam.

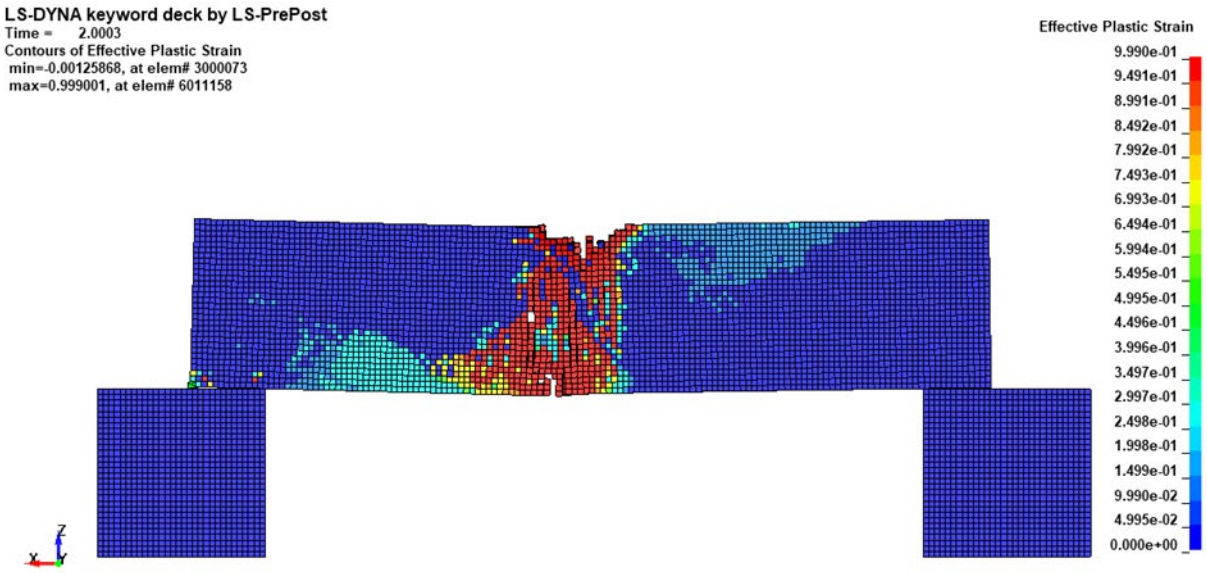

Figure 7.4 Effective plastic strain contour map from CSCM model- drop weight test

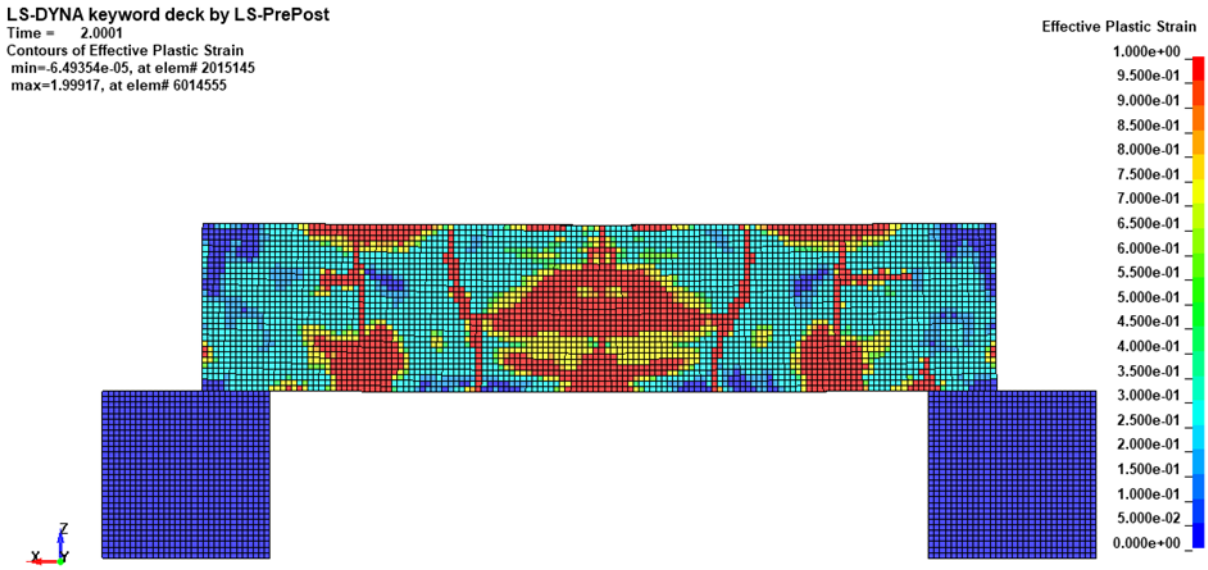

Figure 7.5 Effective plastic strain contour map from K&C model– drop weight test.

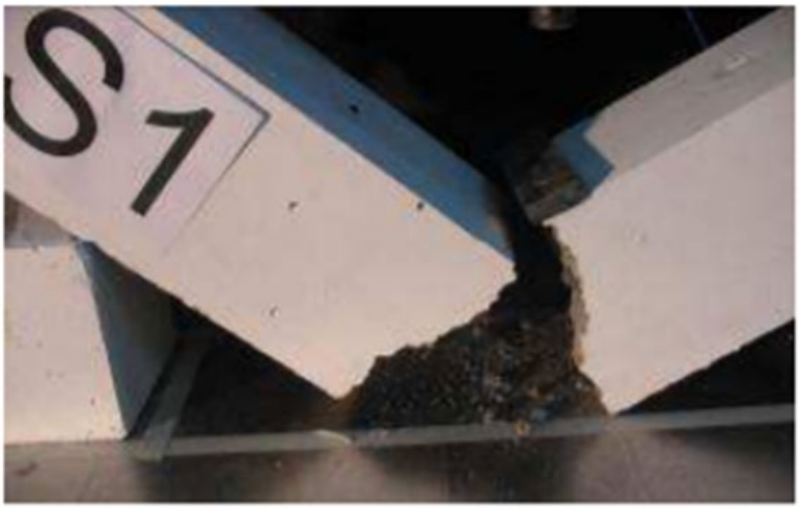

Figure 7.6 Concrete prism after the impact test (Yilmaz et al. 2014)

Chapter 8 Summary and Conclusions

This study simulated the behavior of plain concrete failure in different loading regimes (i.e., quasi-static and dynamic) and under different failure modes (i.e., compression, shear, and flexure). Although reinforced concrete is the main load carrying system in concrete barrier systems, the behavior of plain concrete still needs to be better investigated in order to optimize the design parameters for the barrier systems. Two plasticity-damage based concrete models (i.e., CSCM_CONCRETE and CONCRETE_DAMAGE_REL3 (K&C)) were examined as candidate concrete material models. Simulation results showed that both models can potentially be used for simulation of concrete barrier systems under impact; however some variations were observed between the models. The following concluding remarks can be made:

- Compressive strength, which is the most important property of plain concrete and plays an important role in the design of reinforced concrete, was well predicted by the CSCM and K&C models. However, post-failure behavior was different in the CSCM and K&C models. The CSCM model exhibited more of a ductile behavior, while the K&C displayed more of a brittle behavior. This difference was observed in both of the single element modeling and the full-body simulation of quasi-static tests.
- Flexural and shear strength of plain concrete were also compared between experimental and simulation results, which showed that flexural strengths between the two models were similar and close to experimental results. In shear, both models could not capture accurate behavior, although shear strength from the CSCM model was closer to the experimental results (approximately 12% error).

- Comparison of CSCM and K&C plastic strain contours in quasi-static tests showed that the damaged zones were captured dissimilarly. In general, the K&C model predicted higher rates of plastic strain.
- CSCM and K&C models generated different responses in explicit and implicit analyses. In the uniaxial compression, the best validation results were generated with implicit solver for the CSCM model, while the K&C model produced the better prediction with explicit solver.
- Regarding the drop weight impact test simulation, the CSCM model predicted the behavior of concrete (peak force, acceleration, and damaged zone) better than K&C model.
- Overall, between the two plasticity-damage based concrete models examined in this study, the CSCM material model, although it is limited, appeared more promising to be used for predicting damage and failure of plane concrete under the both quasi-static and dynamic loading than the K&C model. Moreover, the capability of the CSCM model to display element erosion could provide more realistic localized damage contours.

Bibliography

Abu-Odeh, Akram. 2006. “9 Th International LS-DYNA Users Conference Application of New Concrete Model to Roadside Safety Barriers.”

Borrvall, Thomas. 2009. “A Heuristic Attempt to Reduce Transverse Shear Locking in Fully Integrated Hexahedra with Poor Aspect Ratio.” *Dynamore.De*. https://www.dynamore.de/en/downloads/papers/09-conference/papers/G-I-02.pdf.

Brannon, Rebecca, and Seubpong Leelavanichkul. 2009. “Survey of Four Damage Models for Concrete Constitutive Modeling View Project Statistical Mechanics and Swarm Modeling View Project.” https://doi.org/10.2172/993922.

Buyukozturk, Oral, and Syed Sarwar Shareef. 1985. “Constitutive Modeling of Concrete in Finite Element Analysis.” *Computers and Structures* 21 (3): 581–610. https://doi.org/10.1016/0045-7949(85)90135-X.

Collins, Michael P. et al. 1993. “Structural Design Considerations for High-Strength Concrete.” In *Concrete International 15*, 27–34. https://www.concrete.org/publications/internationalconcreteabstractsportal/m/details/id/4217.

Crawford, JE, Y Wu, HJ Choi, JM Magallanes, S Lan - Karagozian & Case, Undefined Glendale, and Undefined 2012. “Use and Validation of the Release III K&C Concrete Material Model in LS-DYNA.”

Erhart, Tobias. 2011. “Review of Solid Element Formulations in LS-DYNA: Properties, Limits, Advantages, Disadvantages.” *Proceedings of the LS-DYNA Developers’ Forum*, 12–13.

Grote, D. L., S. W. Park, and M. Zhou. 2001. “Dynamic Behavior of Concrete at High Strain Rates and Pressures: I. Experimental Characterization.” *International Journal of Impact*

Engineering 25 (9): 869–86. https://doi.org/10.1016/S0734-743X(01)00020-3.

Hallquist, John. O. 2013. "LS-DYNA® Keyword User's Manual Volume II Material Models." *Livermore, California, USA*.

Jiang, Hua, and Jidong Zhao. 2015. "Calibration of the Continuous Surface Cap Model for Concrete." *Finite Elements in Analysis and Design* 97 (May): 1–19. https://doi.org/10.1016/j.finel.2014.12.002.

Liu, Chang Chun, He Xiang Lü, and Ping Guan. 2007. "Coupled Viscoplasticity Damage Constitutive Model for Concrete Materials." *Applied Mathematics and Mechanics (English Edition)* 28 (9): 1145–52. https://doi.org/10.1007/s10483-007-0902-x.

Lubliner, J., J. Oliver, S. Oller, and E. Oñate. 1989. "A Plastic-Damage Model for Concrete." *International Journal of Solids and Structures* 25 (3): 299–326. https://doi.org/10.1016/0020-7683(89)90050-4.

Malvar, LJ, JE Crawford, JW Wesevich, D Simons - Report No. TR94-14.3, and Undefined 1994. 1994. "A New Concrete Material Model for DYNA3D, Karagozian and Case."

Markovich, Natalia, Eytan Kochavi, and Gabi Ben-Dor. 2009. "Calibration of a Concrete Damage Material Model in LS-Dyna for a Wide Range of Concrete Strengths." *Researchgate.Net*. https://doi.org/10.13140/RG.2.1.3503.4723.

Memon, Darya, Azer Maazoun, Stijn Matthys, and David Lecompte. 2019. "Low-Velocity Impact Behaviour of Plain Concrete Beams."

Murray, Yvonne D. 2004. "Theory and Evaluation of Concrete Material Model 159."

Nemat-Nasser, Sia, and A Shokooh. 1980. "On Finite Plastic Flows of Compressible Materials with Internal Friction." *International Journal of Solids and Structures* 16 (6): 495–514. https://www.sciencedirect.com/science/article/pii/0020768380900025.

Ortiz, Michael. 1985. “A Constitutive Theory for the Inelastic Behavior of Concrete.” *Mechanics of Materials* 4 (1): 67–93. https://doi.org/10.1016/0167-6636(85)90007-9.

Rubin, M. B. 1991. “Simple, Convenient Isotropic Failure Surface.” *Journal of Engineering Mechanics* 117 (2): 348–69. https://doi.org/10.1061/(ASCE)0733-9399(1991)117:2(348).

Salamon, Jerzy, and David W Harris. 2014. “Final Evaluation of Nonlinear Material Models in Concrete Dam Finite Element Analysis Reclamation, Nonlinear Material Models, Concrete Material Models, Finite Element Method 16. SECURITY CLASSIFICATION OF: 17. LIMITATION OF ABSTRACT 18. NUMBER OF PAGES 89 19a. NAME OF RESPONSIBLE PERSON.”

Schwer, Len. 2014. “MODELING REBAR: THE FORGOTTEN SISTER IN REINFORCED CONCRETE MODELING.” http://sce.umkc.edu/blast-prediction-contest/.

Schwer, Leonard E. 2005. “SIMPLIFIED CONCRETE MODELING WITH *MAT_CONCRET_DAMAGE_REL3.”

Shah, SP, JGM Van Micr, … N Banthia - Materials and, and Undefined. 2000. “Test Method for Measurement of the Strain-Softening Behaviour of Concrete under Uniaxial Compression.” *Scholars.Northwestern.Edu*. https://www.scholars.northwestern.edu/en/publications/test-method-for-measurement-of-the-strain-softening-behaviour-of-.

Simo, J. C., and J. W. Ju. 1989. “Strain- and Stress-Based Continuum Damage Models-I. Formulation.” *Mathematical and Computer Modelling* 12 (3): 378. https://doi.org/10.1016/0895-7177(89)90117-9.

Willam, Kaspar. 1975. “Constitutive Model for the Triaxial Behaviour of Concrete.” *Intl. Assoc. Bridge Structl. Engrs*. https://ci.nii.ac.jp/naid/10007462496/.

Winkelbauer, Bradley J, Ronald K Faller, Robert W Bielenberg, Scott K Rosenbaugh, John D

Reid, and Jennifer D Schmidt. 2016. “Phase I Evaluation of Selected Concrete Material in LS-DYNA,” April.

Yilmaz, M C, Ö Anil, B Alyavuz, and E Kantar. 2014. “Load Displacement Behavior of Concrete Beam under Monotonic Static and Low Velocity Impact Load.” *International Journal of Civil Engineering*. Vol. 12.

Yonten, Karma, Majid T. Manzari, D. Marzouqui, and A. Eskandarian. 2005. “An Assessment of Constitutive Models of Concrete in the Crashworthiness Simulation of Roadside Safety Structures.” *International Journal of Crashworthiness* 10 (1): 5–19. https://doi.org/10.1533/ijcr.2005.0321.